# INVESTIGATION OF THE EFFECT OF GRAPHENE LAYERS ON MAGNON POLARITON SPECTRUM IN MAGNETIC SUPERLATTICES

**2024**
**MASTER THESIS**
**PHYSICS**

**Hiba ELHARKATI**

**Thesis Advisor**
**Prof. Dr. Rehile ASKERBEYLİ**

# INVESTIGATION OF THE EFFECT OF GRAPHENE LAYERS ON MAGNON POLARITON SPECTRUM IN MAGNETIC SUPERLATTICES

**Hiba ELHARKATI**

**Thesis Advisor**
**Prof. Dr. Rehile ASKERBEYLİ**

**T.C.**
**Karabük Üniversitesi**
**Institute of Graduate Programs**
**Department of Physics**
**Prepared as**
**Master Thesis**

**KARABÜK**
**June 2024**

I certify that in my opinion the thesis submitted by Hiba ELHARKATI titled "INVESTIGATION OF THE EFFECT OF GRAPHENE LAYERS ON MAGNON POLARITON SPECTRUM IN MAGNETIC SUPERLATTICES " is fully adequate in scope and in quality as a thesis for the degree of Master of Science.

Prof. Dr. Rehile ASKERBEYLİ .....
Thesis Advisor, Department of Physics

This thesis is accepted by the examining committee with a unanimous vote in the Department of Physics as a Master of Science thesis. June 28,2024

| **Examining Committee Members (Institutions)** | **Signature** |
|---|---|
| Chairman : Prof. Dr. Rehile ASKERBEYLİ (KBU) | ..... |
| Member : Prof. Dr. Serap SAFRAN (AU) | ..... |
| Member : Assist. Prof. Dr. Ulvi KANBUR (KBU) | ..... |

The degree of Master science by the thesis submitted is approved by the Administrative Board of the Institute of Graduate Programs, Karabuk University.

Assoc. Prof. Dr. Zeynep ÖZCAN. .....
Director of the Institute of Graduate Programs

*"I confirm that all the content in this thesis has been collected and presented following academic standards and ethical guidelines. I have appropriately cited all sources that are not originally my own work, as required by these standards and guidelines."*

Hiba ELHARKATI

## ABSTRACT

**M.SC.Thesis**

**INVESTIGATION OF THE EFFECT OF GRAPHENE LAYERS ON MAGNON POLARITON SPECTRUM IN MAGNETIC SUPERLATTICES**

**Hiba ELHARKATI**

**Karabük University**
**Institute of Graduate Program**
**Department of Physics**

**Thesis Advisor:**
**Prof. Dr. Rehile ASKERBEYLİ**
**June 2024, 55 pages**

This study researches into the effect of graphene layers on magnon polariton spectrum in magnetic superlattices using Maxwell's electromagnetic theory. The high thermal conductivity, exceptional electron transport properties and outstanding mechanical strength of graphene induce surface magnon-polariton modes at interfaces with gyromagnetic media. They result in the localization and dispersion of magnon polaritons.

Magnetic superlattices made up of alternate nanoscale thick materials have unusual electronic, optical and magnetic responses. In particular, this study discusses how these properties are affected by the inclusion of graphene monolayers into a system focusing mainly on the magnon polariton spectrum.

Key findings show that through Fermi energies, graphene can regulate the localization as well as group velocities of magnon polaritons leading to both bulk and surface modes in ferromagnetic crystals. This fact has major implications for developing new spintronic devices that rely on the use of magnon polaritons for information storage and processing.

The present research contributes to knowledge about electromagnetic interactions in nano-scale multilayers magnetic structures as well as reveals possible ways to enhance the functional properties of such systems with graphene. The outcomes from this examination lead to the development of new types of material science research and spintronic technologies.

**Keywords:** Graphene layers, Magnon polariton, Magnetic superlattice, Maxwell's Electromagnetic theory, Surface magnon-polariton modes, Fermi energies, Electromagnetic interaction, Dispersion relation.

**Science Code:** 20205.

# ÖZET

**Yüksek Lisans Tezi**

**MANYETIK SÜPERÖRGÜLERDE GRAFEN KATMANLARININ MAGNON POLARITON SPEKTRUMU ÜZERINDEKI ETKISININ İNCELENMESI**

**Hiba ELHARKATI**

**Karabük Üniversitesi**
**Lisansüstü Eğitim Enstitüsü**
**Fizik AnaBilim Dalı**

**Tez Danışmanı:**
**Prof. Dr. Rehile ASKERBEYLİ**
**Haziran 2024, 55 sayfa**

Bu tezde, Maxwell'in elektromanyetik teorisini kullanarak manyetik süperörgülerde grafen katmanlarının magnon-polariton spektrumu üzerindeki etkisini incelenmektedir. Yüksek ısı iletkenliği, süperiletken elektron taşıma özellikleri ve grafenin süperiletken direnci, manyetik ortamla arayüzlerde yüzey magnon-polariton modlarını indükler. Bu, magnon-polaritonların lokalizasyonuna ve dağılmasına yol açar.

Birkaç nanometre kalınlığında değişen manyetik malzemelerden oluşan manyetik süperörğüler, olağandışı elektronik, optik ve manyetik tepkiler sergiler. Bu çalışma, esas olarak magnon-pola riton spektrumuna odaklanarak, bu özelliklerin grafen tek tabakalarının dahil edilmesinden nasıl etkilendiğini incelemektedir.

Ana keşifler, Fermi enerjileri sayesinde grafenin, magnon-polaritonların konumunun yanı sıra grup hızlarını da düzenleye bileceğini ve manyetik kristallerde yüzey ve hacim modlarına yol açabileceğini gösteriyor. Bunun, bilginin depolanması ve işlenmesi için magnon-polaritonların kullanımına dayanan yeni spintronik cihazların geliştirilmesi için önemli etkileri vardır.

Bu araştırma, nano ölçekli çok katlı manyetik yapılardaki elektromanyetik etkileşimlerin bilgisine katkıda bulunur ve bu sistemlerin grafen ile işlevsel özelliklerini iyileştirmenin olası yollarını ortaya çıkarır. Bu çalışmanın sonuçları, malzeme bilimi ve spintronik teknolojilerinde yeni araştırmaların önünü açmaktadır.

**Anahtar Kelimeler:** Graphene katmanları, Magnon polariton spektrumu, Elektromanyetik teori, Fermi enerjileri, Hacimsel ve yüzeysel modlar, Manyetic etkilesimler.

**Bilim Kodu:** 20205.

## ACKNOWLEDGMENT

First and foremost, I would like to express my heartful gratitude to my advisor, Prof.Dr.Rehile ASKERBEYLI from Karabuk University, for her unwavering support during my Master's studies and research.

**CONTENTS**

**Page**

**Page**

**Page**

## LIST OF FIGURES

**Page**

## SYMBOLS AND ABBREVIATIONS INDEX

### SYMBOLS

T : Temperature

Ɛ : Dielectric constant

$\hbar$ : Planck's constant $\frac{\hbar}{2\pi}$

ω : Angular frequency

$\epsilon 0$ : Permittivity

σ : Electrical conductivity

γ : Gyromagnetic ratio

μ : Magnetic permeability

$H_0$ : External magnetic field

$M_0$ : Magnetization

k : Wavevector

λ : Wavelength

$E_F$ : Fermi energy

$\omega_{m2}^{(M_nF_2)^*}$ : Magnetostatic frequency in MnF2

### ABBREVITIONS

TE: Transverse Electric

TM: Transverse Magnetic

SM: Surface Mode

AF: Antiferromagnetic

FM: Ferromagnetic

EM: Electromagnetic

# PART 1

# INTRODUCTION

## ELECTROMAGNETIC THEORY

Electromagnetic theory is a crucial aspect of modern physics that explains the basic principles that regulate the interaction of electric and magnetic fields [1]. This theory offers a profound comprehension of various natural phenomena, including light, radio waves, electronics, electricity, communication, and power generation. Maxwell's equations, established by James Clerk Maxwell in the 19th century, are the fundamental principles of this theory. The provided equations illustrate how charges and currents produce electric and magnetic fields, as well as their subsequent propagation across space [2]. Maxwell's equations integrated the concepts of light, electricity, and magnetism, providing a unified explanation for previously inexplicable phenomena. Additionally, these equations accurately predicted the presence of electromagnetic waves that propagate at the speed of light [3]. This revolutionary discovery opened doors for other technological progressions, including the emergence of wireless communication, radar, and contemporary electrical engineering [4]. Furthermore, electromagnetic theory remains essential in advanced research fields such as quantum electrodynamics and photonics.

The following paragraphs will delve into a topic of significant interest within this field: the effect of graphene layers on the magnetic polariton spectrum in magnetic superlattices. My previous studies have explored this topic in detail, providing insights into the interaction mechanisms and potential applications of this phenomenon.

**Graphene layers** consist of carbon atoms organised in a hexagonal honeycomb with each layer being only one single atom thick. They are bonded together with strong sp2 bonds and exhibit unique properties like high thermal conductivity, exceptional electron transport characteristics, and remarkable mechanical strength. Graphene is typically produced from graphite oxide, making it hydrophilic, meaning it readily interacts with and disperses in water. This unique material possesses extraordinary properties and holds immense potential for various applications across diverse fields.[5,6]

When graphene is positioned at the interface between a vacuum and a gyromagnetic medium generates surface magnon polariton modes, these modes typically have frequencies in the range of few (Ghz), influencing their localization and dispersion relations.[7]

**Superlattices** are structures made up of alternating layers of different materials, usually with thicknesses on the nanoscale [8]. They are designed to exhibit unique electronic, optical, and magnetic properties that are not found in the individual constituent materials. And used in various fields of research and technology owing to their unique properties and potential applications [9]**.** Here are some key points about superlattices:

Understanding the behavior of superlattices is important for advancing materials science and developing new technologies [10]

**Magnon-polaritons** are bulk and surface modes in ferromagnetic crystals, and their concentration and carrier velocities are affected by the presence of graphene [11]**.** When light interacts with a magnetic material confined between graphene sheets, it can excite special waves called magnons. These magnons can then couple with the light. This phenomenon has potential applications in the development of new types of spintronic devices that use magnon-polaritons for information storage and processing [12].

The magnon polariton spectrum in magnetic superlattices has been studied in several papers. Liao et al. illustrate valley-selective phonon-magnon scattering in magnetoelastic superlattices, where the lattice symmetry and magnetization control the nonreciprocity of transmission [13]**.** Vasconcelos and Cottam investigate the influence of graphene sheets on surface and bulk magnon-polaritons in magnonic crystals, showing that the Fermi energies in graphene can control the localization and group velocities of the modes [14]. Ta et al. also study magnetophonon polaritons in superlattices consisting of alternating antiferromagnetic and ion-crystal components, finding various bulk polariton bands with negative and positive refraction and various surface polariton modes [15] Tagiyeva and Tanatar derive the general expression for surface-guided magnetic polaritons in antiferromagnetic superlattices containing impurity films, showing the reciprocal nature of the spectrum and the presence of both strongly and weakly localized modes [16]**.** Ignatchenko and Tsikalov studied the spin-wave spectrum in periodic superlattice of one-dimensional magnon crystals', calculating the band gaps based on the magnetic parameter differences and layer thickness ratios [17]**.**

After establishing the significance of the magnon polariton spectrum in magnetic superlattices in the introduction, it is crucial to delve deeper into the foundational concepts of magnetic properties of materials and Maxwell's electromagnetic theory. Understanding these concepts will provide essential groundwork for exploring the interaction between magnons and electromagnetic fields in nanoscale magnetic structures.

In this section, we will first explore the diverse magnetic behaviors exhibited by different materials, ranging from diamagnetism and paramagnetism to ferromagnetism and beyond. This discussion will shed light on the fundamental principles governing magnetic interactions and the factors influencing magnetization in materials.

# PART 2

# MAGNETIC PROPERTIES OF MATERIALS

Materials have a wide range of magnetic l characteristics that can be classified based on the way they react to magnetic fields. Diamagnetic materials show a weak tendency to repel, paramagnetic materials present a minor inclination towards attraction while ferromagnetic substances exhibit strong attraction and tend to retain magnetism. The magnetism at the microscopic level is explained by quantum mechanics in terms of electron currents creating magnetic moments that explains why there are magnets [18]**.** Forces can be exerted on dipoles, particle alignment, and production of magnetic structures through the interaction between matter and magnetic fields [19].Carbon, manganese silicon, and other impurities could affect magnetic properties such as iron, nickel cobalt, etc., which are ferromagnetic metals. These factors determine parameters such as hysteresis loss and permeability [5] People have known for many years that some objects are attracted to or pushed away from others since ancient times when man discovered stones like magnetite being the first natural magnets [20]**.**

## 2.1. VARIOUS SUBSTANCES EXHIBIT SEVERAL TYPES OF MAGNETIC BEHAVIOR. HERE ARE THE MAIN ONES

### 2.1.1. Diamagnetism

Diamagnetic substances include noble gases, ionic compounds, and semiconductors with robust covalent bonding. Electrical charges in all such substances tend to protect the internal regions of the body from magnetic fields. Hence, it has a small negative value and is referred to as susceptibility (Figure 2.1). The phenomenon arises due to the precession

of electronic orbits around the direction of the applied magnetic field. The precession is against the external field induction causing slightly negative susceptibility [21,22].

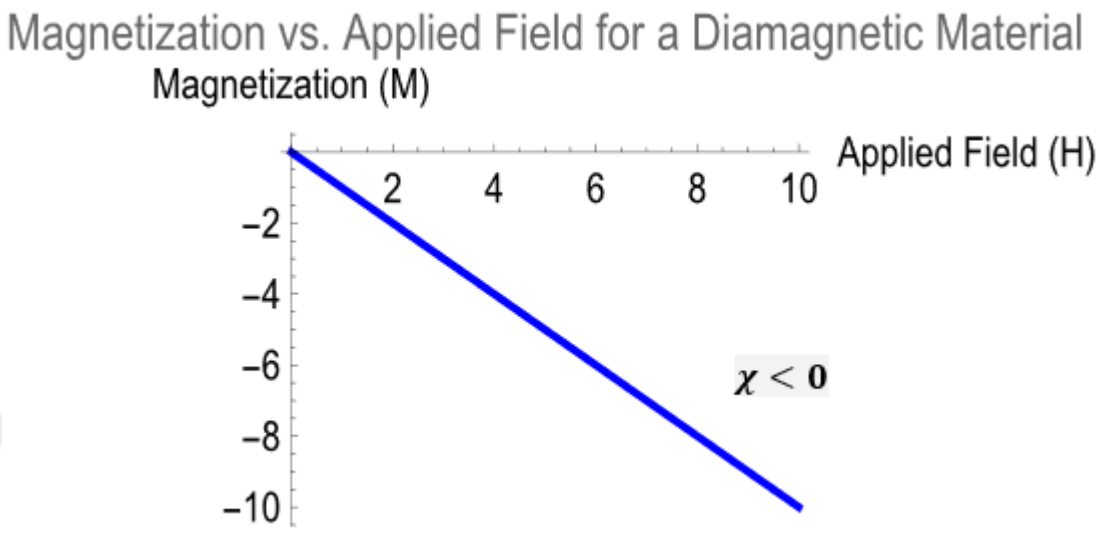


Fig. 2. 1. Magnetisation versus applied field for a diamagnetic material

The unique type of diamagnets that have $\chi = -1$ are ideal superconducting materials. Therefore, they push away magnetic fluxes in their state of superconductivity.

Diamagnetism is a property that can be observed in every molecule or atom in every case. Nevertheless, this effect is very weak and cannot be seen because it is always negligible compared to how atomic magnetic moments behave when faced with an external field on other materials [23,24].

### 2.1.2. Paramagnetism

If we take a group of individual atoms and see them. We will find that each of them has a magnetic moment, and between them the interaction is minimal, Their minimal interaction classifies them as atomic magnets. They possess the liberty to align themselves in any direction they choose. At room temperature, thermal energy causes the orientations of these magnetic atoms to become randomized.

Thus, when there is no external magnetic field, the overall magnetization is equal to zero, represented as: $M = \Sigma m = 0$

However, upon applying an external magnetic field, In the presence of a magnetic field, certain atomic magnetic moments rotate and align themselves along the direction of the field. This alignment leads to a slight net magnetization and positive susceptibility $(\chi)$. As the applied field strength increases, a greater number of atomic moments align themselves with the external field. This results in a proportional increase in M, while chi remains constant. If the magnetic field remains constant as the temperature increases, the increase in thermal agitation leads to a decrease in $M$ (magnetization) and (magnetic susceptibility). The relationship shown in Figure 1.2 demonstrates that susceptibility and temperature are inversely related, which is referred to as the Curie's law of paramagnetism. Paramagnetism in metals, such as aluminum, is generally feeble and similar to the typical diamagnetic properties. Practical measurements have difficulties due to the presence of even small amounts of ferromagnetic contaminants, such as iron in parts per million, which can lead to inaccurate results[25].

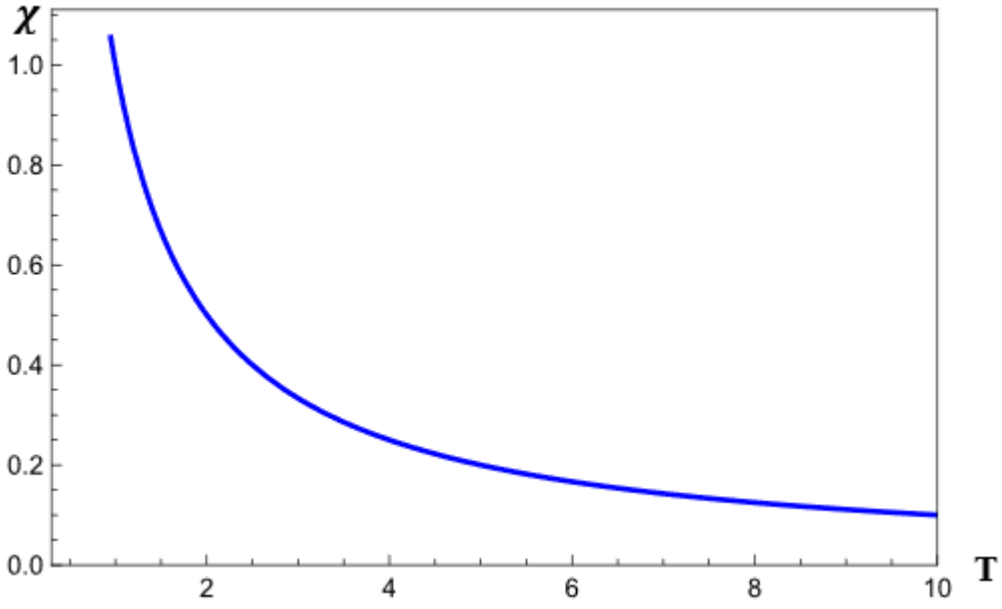


Fig. 2. 2. X vs T illustrates the Cruie law of

### 2.1.3. Ferromagnetism

In ferromagnetism, individual atoms possess a net magnetic moment. This is enhanced by a strong but short-range interaction between neighboring atoms, causing their magnetic moments to align positively in parallel. This alignment can be either in the ↑↑ or →→ direction [26,27].

This is not the same as dipolar forces; it's a stronger, shorter-range effect called exchange that comes from quantum physics [28]. Within uniform magnetization zones, magnetic moments automatically align to establish a net magnetization. Subsequently, they orient in a manner that minimizes the net magnetization of the material[29].

The way these substances react to outside magnetic fields is not linear (see Figure. 2.3), and they show hysteresis. This means that their behavior is affected by their magnetic past as well as their microstructural and extrinsic properties.

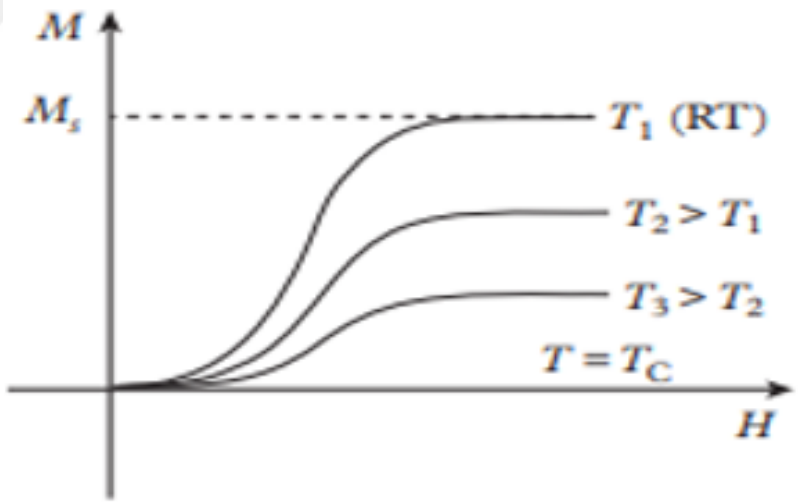


Fig. 2.3. The initial magnetization of a ferromagnet varies with the applied magnetic field and temperature.

In fact, if the direction of the magnetic field is reversed, the magnetization does not follow the same path as the dependence on the field, which means( ***M*** is not a one-valued function ***H***).This hysteresis is a characteristic feature of ferromagnetic and

ferromagnetic materials. When a strong external magnetic field is applied, the magnetic moments in all fields align in the same direction, which causes the material to become fully magnetized in the direction of the applied field. Saturation magnetization, represented by MS, is the maximum magnetization that a material can achieve when exposed to strong magnetic fields [30].

As temperature rises, the hysteresis behavior remains consistent, but the saturation magnetization decreases until reaching a critical threshold. At this point, thermal energy overcomes the strong interaction between neighboring magnetic moments. At the Curie temperature ($T_c$), the material's saturation magnetization drops to zero. The Curie temperature reflects the strength of interaction between atomic magnetic moments. When the temperature ($T$) exceeds $T_c$, the material exhibits paramagnetic properties and follows the Curie-Weiss law of ferromagnetism (see Figure 2.4).

$$\chi = \frac{c}{T - T_c} \tag{2.1}$$

The magnetic susceptibility, χ, exhibits an infinite increase as the temperature nears to the temperature of Curie, $T_c$. It exhibits paramagnetic behaviour. However, caution is necessary. For a ferromagnet, The applied magnetic field $\boldsymbol{H_{app}}$ minus the demagnetizing field $\boldsymbol{N_d M}$. is used to find the internal magnetic field, $\boldsymbol{H_{in}}$

$$\boldsymbol{H_{in} = H_{app} - N_d M} \tag{2.2}$$

The intrinsic susceptibility of the material, $\boldsymbol{\chi_{mat}}$, diverges at the critical temperature, $Tc$. The magnetic susceptibility of a material is equal to the ratio of its magnetization ($M$) to its internal magnetic field $\boldsymbol{H_{in}}$.

$$\boldsymbol{\chi_{mat} = M / H_{in}} \tag{2.3}$$

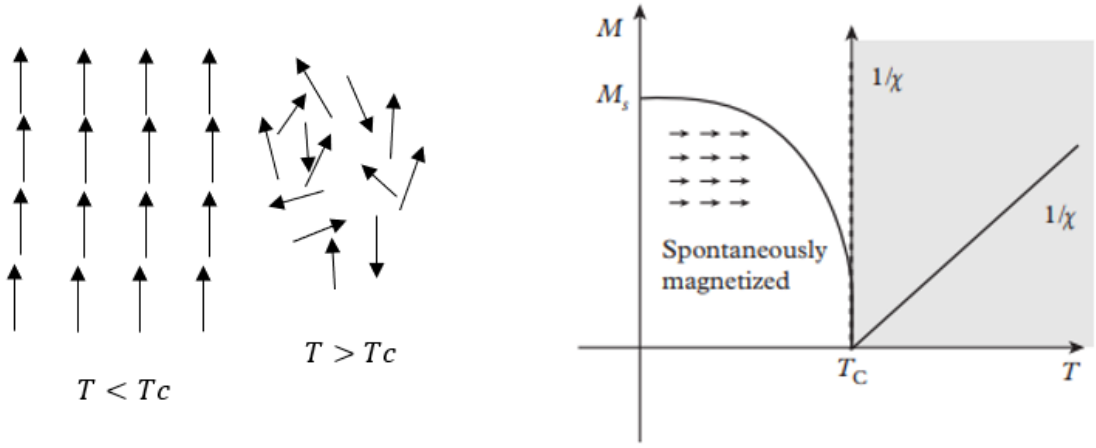


Fig. 2.4. Variation of magnetization in a ferromagnet concerning temperature beyond the Curie temperature, $T_c$

When susceptibility is tested in an experiment, it depends on the sample,

$\boldsymbol{\chi_{sample} = M/H_{app}}$, and is directly associated with $\boldsymbol{\chi_{mat}}$ as

$\boldsymbol{\chi_{sample} = \chi_{mat}/(1 + N_d\chi_{mat})}$

When $T_c$ is approached from above, the experimentally observed susceptibility (χ) of the sample rises by just $\boldsymbol{1/N_d}$

### 2.1.4. Antiferromagnetism

In antiferromagnetic materials, atoms display significant magnetic properties while also experiencing strong repulsive interactions. As a result, adjacent magnetic moments typically align in opposite directions. Additionally, the crystal structure features a unique magnetic component that is evenly distributed across two interlinked but opposing lattices. It also ensures that there is no overall or spontaneous magnetization when the magnetic moments are properly oriented [31].

At standard temperatures, Several of these materials demonstrate paramagnetic characteristics. Nevertheless, when the temperature drops below a certain level, called the Néel temperature ($T_N$), these materials show a sudden and marked change in their susceptibility. Moreover, the susceptibility of the material below the $T_N$ is affected by its orientation and depends on when the magnetic field is applied perpendicular ($\boldsymbol{H}_{\perp}$) or parallel ($H$) to the chosen spin-lattice direction,as illustrated in (Figure 2.5).

Theoretically, the susceptibility $\chi$ of an antiferromagnet for $T > T_N$ is Defined in mathematical terms as :

$$\chi = \frac{C}{T - \theta} = \frac{C}{T + T_N} \tag{2.4}$$

Here: $\theta = - T_N$ is the intercept of $1/\chi$ when extrapolated to dhe temperature axis for $T > T_N$.

### 2.1.5.Ferrimagnetism

This phenomenon, frequently seen in several substances such as oxides, involves multiple magnetic species on distinct sub-lattices, each with a unique magnetic moment. These sub-lattices interact strongly and antagonistically, causing their magnetic moments to align in opposite directions [31]. Unlike antiferromagnets, Ferrimagnets exhibit inherent magnetism below the Curie temperature ($T_c$) when the sub-lattices are organised in a certain sequence.[32] (Figure 2.5).

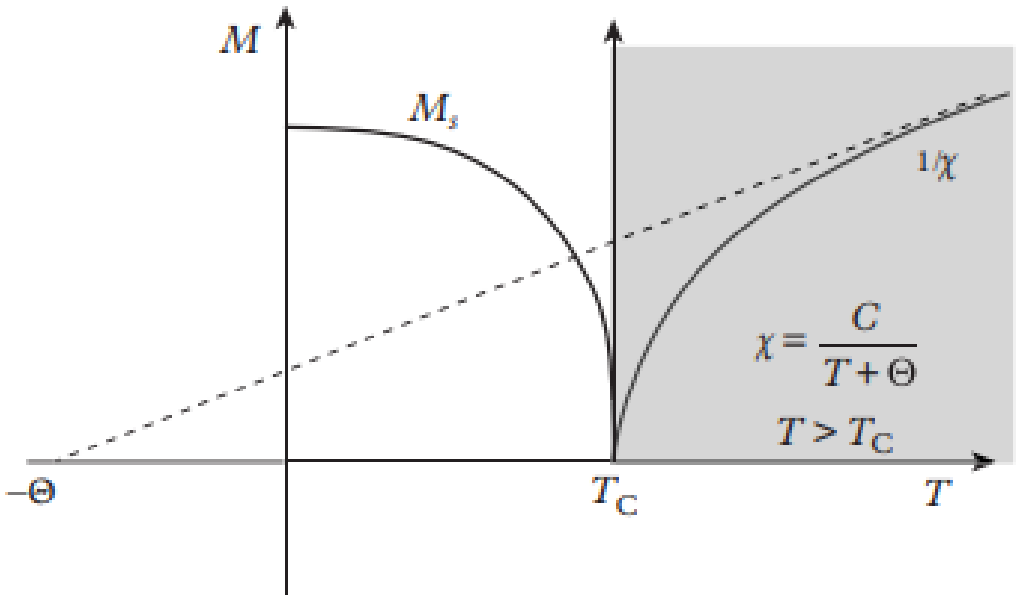


Fig. 2.5. The interaction between magnetism and temperature in a ferrimagnetism.

### 2.1.5. Hysteresis

Ultimately, we conduct a concise examination of the response of magnetization and magnetic induction seen in both ferromagnetic and ferrimagnetic materials. Although a block of ferromagnetic material naturally possesses magnetism, the magnetization of the material can be disturbed by the existence of magnetic domains. These domains correspond to distinct areas within the material, each having its own magnetic properties defined by the magnetization value ($Ms$). N nevertheless, their diverse orientations result in minimal contribution to the overall net magnetism.

When exposed to a positive magnetic field and subsequently reduced, the material's magnetization does not go back to its original state. Hysteresis is the phenomena where a sequence of "minor" loops are created by gradually increasing and then reversing the applied magnetic fields. (Figure 2.6)a illustrates the hysteresis curve, which is the broadest range that includes all minor loops for the ferromagnetic material. This curve arises when the material becomes fully saturated in the presence of a sufficiently powerful magnetic field. The saturation magnetization symbol ($Ms$) represents the highest achievable level of magnetization [33]. Furthermore,, the maximum value of $Ms$, referred to as $M0$, is fofoundt the temperatur of absolute zero ($0\ K$), taking into account the influence of temperature.

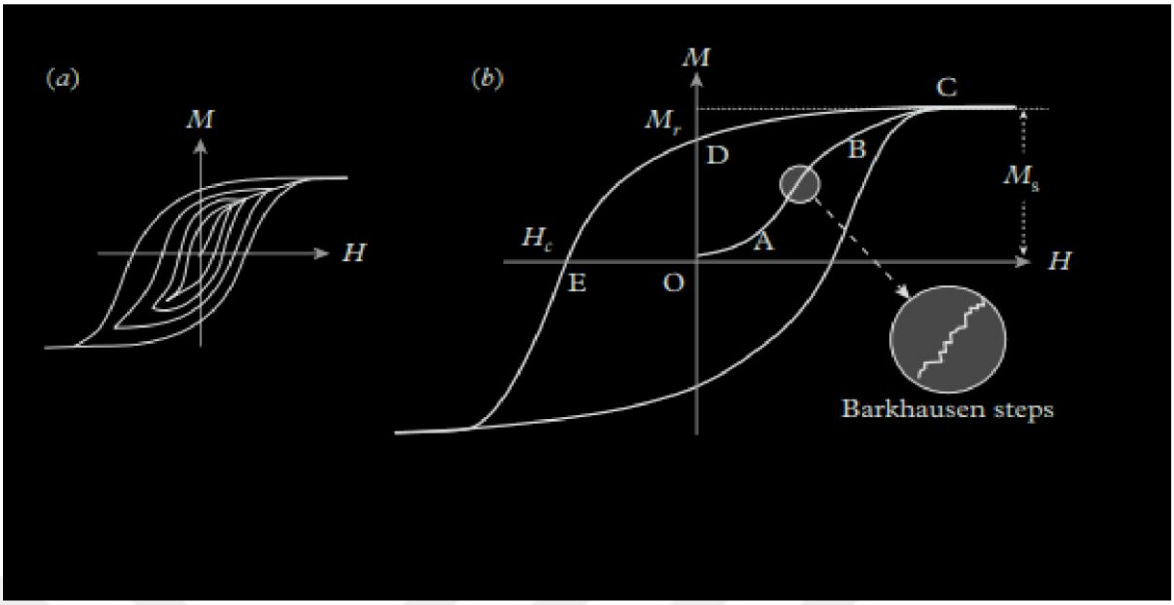


Fig. 2.6. a) A sequence of smaller loops achieved by progressively raising the maximum applied field. The hysteresis curve represents the envelope of these tiny loops. (b) A typical hysteresis loop for a ferromagnet illustrating key areas of interest.

## 2.2.MAXWELL EQUATIONS

Maxwell formulated the relationship between electricity and magnetism in mathematical terms, describing the inter-relationship between the electric field, $(\vec{E})$, the magnetic induction, $(\vec{B})$, the charge density, $\rho$, and the current density, $(\vec{J})$.

In free space, with permittivity, $\varepsilon_0$, the first of his four equations is :

$$\nabla \cdot \vec{E} = \frac{\rho}{\varepsilon_0} \tag{2.2.1}$$

This is a reformulation of the Coulomb law and states that every line of electric field originates on (or diverges from) a positive charge and ends on (or converges into) a negative charge.

The second equation:

$$\nabla \cdot \vec{B} = 0 \tag{2.2.2}$$

The second equation is given by the divergence of the magnetic field, indicating that, Unlike electric charge, magnetic fields do not have discrete sources or sinks. Only currents can generate magnetic fields. In essence, this implies that magnetic monopoles are non-existent; the magnetic field lines must form unbroken loops and cannot initiate or terminate at any location. In contrast, electric fields have the ability to both originate from and terminate at electric charges.

The third and fourth equations of Maxwell's equations address the flow of electric fields and the generation of magnetic induction. Faraday's law of electromagnetic induction states that electric fields form closed loops around regions with a varying magnetic field, which can be mathematically represented as:

$$\nabla \times \vec{E} = -\frac{\partial B}{\partial t} \tag{2.2.3}$$

Recall the Ampere law, which states that in the absence of a changing electric field ($\partial E/\partial t = 0$), loops of the magnetic field are formed around an electrical current. Maxwell generalized this in his fourth equation, including the permeability of free space, $\boldsymbol{\mu_0}$, as :

$$\nabla \times \vec{B} = \mu_0 \vec{J} + \mu_0 \varepsilon_0 \frac{\partial \vec{E}}{\partial t} \tag{2.2.4}$$

Note that $\varepsilon_0 \mu_0 = \frac{1}{c^2}$ , where c is the velocity of light. These equations describe electromagnetic fields in free space. Once we include matter, we have to distinguish between currents that we can measure, $\vec{\boldsymbol{J}}_{free}$ and microscopic bound currents, $\vec{\boldsymbol{J}}_{bound}$, due to circulating electrons in atoms that, in principle, give rise to atomic magnetic moments. The total current is the sum:

$$\vec{\boldsymbol{J}} = \vec{\boldsymbol{J}}_{free} + \vec{\boldsymbol{J}}_{bound} \tag{2.2.5}$$

Moreover, the bound currents are related to the magnetization, $(\vec{M})$ as:

$$\nabla \times \vec{M} = \vec{\boldsymbol{J}}_{bound} \tag{2.2.6}$$

Similarly, (2.2), can be written for the magnetic field $(\vec{H})$, as:

$$\nabla \cdot \vec{H} = -\nabla \cdot \vec{M} \tag{2.2.7}$$

This shows that $\vec{H}$ is different to $\vec{B}$, for it is not divergence-free. Materials may also have an electric polarization, $\vec{P}$, so we write the general electric displacement, $\vec{D}$, as a sum of the electric field and the polarization, as:

$$\vec{D} = \varepsilon_0 \vec{E} + \vec{P} \tag{2.2.8}$$

Therefore, we can present Maxwell's four equations, modified for the presence of matter, distinguishing between bound and free charges as:

$$\nabla \cdot \vec{D} = \rho_{free} \tag{2.2.9}$$

$$\nabla \cdot \vec{B} = 0 \tag{2.2.10}$$

$$\nabla \times \vec{E} = -\frac{\partial \vec{B}}{\partial t} \tag{2.2.11}$$

$$\nabla \times \vec{H} = \vec{J}_{free} + \frac{\partial \vec{D}}{\partial t} \tag{2.2.12}$$

# PART 3

## MAGNETİC POLARITON AND MAGNETIC SUPERLATTICE

The dispersion equations for bulk and surface magnetism in N-layered superlattices are obtained using the 'transfer matrix' method, this method is utilized for the scenarios where.$N = 2$ and $N = 3$, which correspond to distinct magnetic layers in a basic unit. It is assumed that the layers are magnetized in a way that is parallel to both the planes of the film and to each other. The work provides precise formulations for the 'transfer matrix' and the dispersion equations of bulk and surface modes in the Voigt configuration. The wave spectrum of various superlattices composed of ferromagnetic, antiferromagnetic, and non-magnetic materials is demonstrated through the use of multiple numerical examples. The study of collective excitation in magnetic superlattices has gained great attention in recent years. The structures analyzed usually consist of a series of magnetic films separated by a non-magnetic material. Within these structures, spin waves may interact in separate magnetic layers through the long-distance dipole field generated by the motion of the spins. The eigenstates that appear as a result are subsequently organized into teams, representing the collective excitation of the entire SuperNet.The user text is.[34].

### 3.1. MAGNETIC POLARITONS IN THE MAGNETIC SUPERLATTICES

Magnetic polaritons are a type of collective oscillations that arise from the interaction between electromagnetic waves and magnetic moments within a material. These excitations can manifest in diverse systems, such as superlattices comprised of distinct

magnetic materials. The dispersion equations for bulk and surface in superlattices provide a clear understanding of the properties and interactions of magnetic polaritons inside these complex structures [35].

In the context of superlattices:

A magnetic superlattice is a periodic structure composed of alternating layers of different magnetic materials. These materials can be ferromagnetic, antiferromagnetic, or non-magnetic, creating a tailored magnetic configuration within the superlattice [36].

In the structure of the superlattice, the layers are usually magnetized in a parallel manner from the film planes and also parallel to each other.

## 3.2. FERROMAGNETIC SUPERLATTICE

A ferromagnetic superlattice is a periodic structure composed of alternating layers of ferromagnetic materials. These materials exhibit spontaneous magnetization and retain their magnetization even in the absence of an external magnetic field[37].

Ferromagnetic superlattices have a collective magnetic behavior where neighboring magnetic moments align parallel to each other. The magnetic interactions between ferromagnetic layers can lead to phenomena like exchange coupling and magnons, influencing the overall magnetic properties of the superlattice [38].

### 3.3.1. Applications Of Ferromagnetic Superlattice

Ferromagnetic superlattices are utilized in spintronics, magnetic storage devices, and magnetic sensors due to their tunable magnetic properties. The controlled manipulation of magnetization in ferromagnetic superlattices enables the development of novel magnetic devices with tailored functionalities. Studies have investigated the spin wave dispersion and magnetostatic modes in ferromagnetic superlattices to understand their magnetic behavior and potential applications [34].

**For ferromagnetic material**s, the magnetic permeabilities $\mu_\perp$ and $\mu_x$ be utilized in the following form:

$$\mu_\perp = 1 + \frac{\Omega_0\,\Omega_m}{\Omega_0^2-\omega^2} \tag{3.1}$$

$$\mu_x = -\frac{\Omega_m\,\omega}{\Omega_0^2-\omega^2} \tag{3.2}$$

Here $\Omega_0$ is the frequency of the uniform bulk mode, $\Omega_0 = g\mu_0\gamma_0(H_0 + Ha)$ , where $g$, $Ha$ and $\mu_0$, represent the Lande factor, the uniaxial magnetic anisotropy field and the magnetic permeability of the vacuum, respectively. and $\gamma_0$ is defined as $\gamma_0 = e/2m$ ($e$ and $m$ represent the charge and mass, respectively, of an electron with ($e > 0$)). Furthermore the symbole $\Omega_m$ is defined as

$\Omega_m = g\mu_0\gamma_0 M_0$, where $M_0$ represents the spontaneous magnetisation of the substance.

### 3.3. ANTIFERROMAGNETIC UNIAXIAL MATERIALS

$$\mu_\perp = 1 + \frac{\Omega_a\,\Omega_m}{\Omega_1^2-(\omega+g\mu_0\gamma_0H_0)^2} + \frac{\Omega_a\,\Omega_m}{\Omega_1^2-(\omega-g\mu_0\gamma_0H_0)^2} \tag{3.3}$$

$$\mu_x = \frac{\Omega_a\,\Omega_m}{\Omega_1^2-(\omega+g\mu_0\gamma_0H_0)^2} - \frac{\Omega_a\,\Omega_m}{\Omega_1^2-(\omega-g\mu_0\gamma_0H_0)^2} \tag{3.4}$$

where $\Omega_1$ is the frequency of antiferromagnetic resonance when there is no field applied

$$\Omega_1 = g\mu_0\gamma_0\,[Ha(H_a + 2H_e)]^{\frac{1}{2}} \tag{3.5}$$

Where $Ha$ is the anisotropy field and $He$represents the exchange field. The formula for $\Omega_m$ is the same as for ferromagnetic systems but $M_0$ is the sublattice magnetization. I the end , $\Omega_a$ is defined as:

$$\Omega_a = g\mu_0\gamma_0 H_a. \tag{3.6}$$

### 3.4. TYPE OF SUPERLATTICE

**Antiferromagnetic-non-magnetic (AF-N) superlattices**

are characterized by the presence of repeated layers of antiferromagnetic and non-magnetic materials. In these structures, magnetic moments in the antiferromagnetic layers are opposed to each other while those in the non-magnetic layers do not have any magnetic properties. As a result, there is a unique manifestation of their magnetic properties and spin wave dispersion within superlattice.[39].

The occurrence of surface modes on AF/NM interfaces that are not observed in the bulk material is one such consequence [34].

**Antiferromagnetic-antiferromagnetic (AF-AF) superlattices**

consist of alternating layers where different antiferromagnets are used. Special features in the wave spectrum arise from coupling between surface modes in two neighboring antiferromagnets [40]. For example, this interaction can lead to multiple bands of magnetostatic mode and surface mode when anti-ferro-resonance frequency close [41]. The interplay has significant implications for its static and dynamic magnetization properties[34].

**Ferromagnetic-ferromagnetic (F-F) superlattices**:

are composed of alternated ferromagnetic material and have unique characteristics of the wave spectrum [42].

The wave spectrum usually contains two bands for bulk waves associated with surface modes in a ferromagnetic film. These bands differ in frequency range and propagation properties. This interaction between surface modes in the ferromagnetic layers modifies wave properties and by extension, the entire wave spectrum of a superlattice structure [43]

# PART 4

# EFFECTIVE-MEDIUM APPROXIMATION FOR MAGNETIC SUPERLATTIVE

## 4.1. OVERVIEW OF FERROMAGNETIC AND ANTIFERROMAGNETIC RESONANCE FREQUENCIES

Ferromagnetic resonance frequencies often reside inside the microwave range, while antiferromagnetic resonance is frequently found inside the far infrared area. Within this region characterized by high-frequency dispersion, which is of considerable importance, the wavelength in free space is substantially greater than the period of the superlattice $L = a + b$,where $a$ and $b$ represent the measurements of the thicknesses of the magnetic superlattice layers [44].

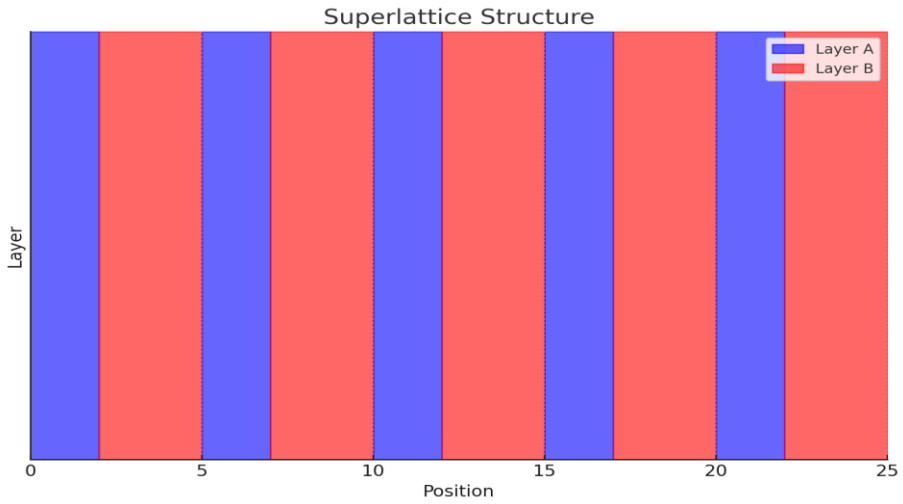


Fig. 4.1. This is a diagram showing the structure of the superlattice. The alternate layers of material A (magnified in blue) and B (highlighted in red) manifest the periodic arrangement characteristic to a superlattice.

.

## 4.2. HIGH-FREQUENCY DISPERSION IN SUPERLATTICES

This implies that with the exception of extremely short frequency gaps near resonance, the wave numbers k in the dispersion equations are significantly less than the inverse of $L^{-1}$ .When faced with such situations, an antiferromagnetic superlattice can be simplified and treated as a uniform anisotropic medium, as explained by Agranovich and Kravtsov [44].

## 4.3. ELECTROMAGNETIC FIELD ANALYSIS IN SUPPERLATICES

In the superlattice shown in (Fig. 4.1). we are examining an rf magnetic field that is oriented in the x-y plane. The wavelength of this field is much longer than the period of the superlattice and is referred to as $L$. Then as a result, the magnetic field **B** and the intensity of the magnetic field **H** are identical in successive layers of Component 1 and successive layers of Component 2.

As one known, the surface magnetic polaritons exist only for transverse electric modes (TE). Thus, for the TE modes in the considered geometry the electric fields E=(0,0,$E_z$ )
in the antiferromagnetic layer *i(i*=1,2) can be written in the following form:

$$E_z^{(i)} = \left(A^{(i)} e^{ik_y y} + C^{(i)} e^{-ik_y y}\right) e^{ik_x x} \qquad \text{…….(4.1)}$$

### 4.3.1. Surface Magnetic Polaritons

Here the index $k_y = i\mathrm{k}_2$ is real for guided modes and imaginary for surface modes. Firstly, using the Amper's law for each SL magnetic medium, we find:

$$\vec{B} = \frac{1}{i\omega} \mathrm{rot}\, \overrightarrow{E} \qquad (4.2)$$

$$\vec{E} = (0,0,E_z)$$

$$\text{rot}\,\vec{E} = \begin{vmatrix} \vec{x} & \vec{y} & \vec{z} \\ \frac{\partial}{dx} & \frac{\partial}{dy} & \frac{\partial}{dz} \\ 0 & 0 & E_z \end{vmatrix} = \vec{x}\frac{dE_z}{\partial y} - \vec{y}\frac{dE_z}{\partial x}$$

$$\mathbf{rot}\,\vec{E} = \vec{x}ik_y\left(Ae^{ik_y y} - Ce^{-ik_y y}\right)e^{ik_x x} - \vec{y}ik_x\left(Ae^{ik_y y} + Ce^{-ik_y y}\right)$$

After some algebra one can derive the expressions for **B:**

$$B_x^{(i)} = \frac{k_y}{\omega}\left(Ae^{ik_y y} - Ce^{-ik_y y}\right)e^{ik_x x} \tag{4.3}$$

$$B_y^{(i)} = -\frac{k_x}{\omega}\left(Ae^{ik_y y} + Ce^{-ik_y y}\right)e^{ik_x x} \tag{4.4}$$

### 4.3.2. Effective Medium Permeability Tensor

Then, consider the equation $\vec{B} = \mu_0\mu\vec{H}$, one can written the expressions for $H_x$ and $H_y$ In each layers:

$$H_x = \frac{1}{\mu'\omega}\left(\Lambda_- e^{ik_y y} + \Lambda_+ Ce^{-ik_y y}\right)e^{ik_y y}\, e^{-i\omega t} \tag{4.5}$$

$$H_y = -\frac{1}{\mu'\omega}\left(\Lambda_- e^{ik_y y} + \Lambda_+ Ce^{-ik_y y}\right)e^{ik_x y}\, e^{-i\omega t} \tag{4.6}$$

Where $$\Lambda_\pm = \pm k_y y - i\mu_{xy}k_x \tag{4.7}$$

$$\mu' = \left(\mu_{xy}\right)^2 - \mu_{xx}\mu_{yy} \tag{4.8}$$

### 4.3.3. Dispersion Relations For Magnetic Polaritons In Effective Medium

In the context of of effective -medium approximation, and applying the electromagnetic boundary conditions for antiferromagnetic superlattice, we have :

$$\langle H_x \rangle = H_x^{(1)} = H_x^{(2)} \tag{4.9}$$

$$\langle B_y \rangle = B_y^{(1)} = B_y^{(2)} \tag{4.10}$$

It is well-known that ferromagnetic resonance frequencies often be within the microwave frequency range, while antiferromagnetic resonance frequencies are frequently found in the far infrared region. Now we are considering an RF (radio frequency) magnetic field that is situated in the x-y axis of the superlattice with the wavelength of the RF magnetic field is significantly bigger than the period of the superlattice. This means that over the scale of one period, the fields can be assumed to be approximately constant. The boundary conditions for the magnetic field ($H_x$) and the magnetic induction ($B_y$) must be consistent throughout the interfaces between layers. Thus, these components can be regarded as their layer-average values $\langle \overrightarrow{H_x} \rangle$ and $\langle \overrightarrow{B_x} \rangle$ [44].

$$\langle Bx \rangle = \frac{aB_x^{(1)} + bB_x^{(2)}}{a+b} \tag{4.11}$$

$$\langle Hy \rangle = \frac{aH_y^{(1)} + bH_y^{(2)}}{a+b} \tag{4.12}$$

consider the equations (4.4-4.6) and the reorganized gives relations in terms of the effective -medium permeability tensor:

$$\begin{bmatrix} \langle B_x \rangle \\ \langle B_y \rangle \end{bmatrix} = \mu_0 \begin{bmatrix} \bar{\mu}_{xx} & \bar{\mu}_{xy} \\ \bar{\mu}_{yx} & \bar{\mu}_{yy} \end{bmatrix} \begin{bmatrix} \langle H_x \rangle \\ \langle H_y \rangle \end{bmatrix} \tag{4.13}$$

$$\langle B_x \rangle = \left( \frac{f_a \mu_v^1}{\mu_{x_x}} + \frac{f_b \mu_v^2}{\mu_{xx}^2} \right) \langle H_x \rangle + \left( \frac{i\mu_{xy}^2}{\mu_{xx}^1} f_a + \frac{i\mu_{xy}^2}{\mu_{xx}^2} f_b \right) \langle B_y \rangle \tag{4.14}$$

$$\langle H_y \rangle = \left[ \frac{f_a}{\mu_{xx}^1} + \frac{f_b}{\mu_{xx}^2} \right] \langle B_y \rangle + \left( f_a \frac{i\mu_{xy}^2}{\mu_{xx}^1} + f_b \frac{i\mu_{xy}^2}{\mu_{xx}^2} \right) \langle H_x \rangle \tag{4.15}$$

Here $f_a = \frac{a}{a+b}$ and $f_b = \frac{b}{a+b}$

And

$$\langle \mu_{xy} \rangle = \frac{f_{a1}\mu_{xy}^{1}\mu_{xx}^{2}+f_{b1}\mu_{xy}^{2}\mu_{xx}^{1}}{f_{a1}\mu_{xx}^{2}+f_{b1}\mu_{xx}^{1}} \quad (4.16)$$

$$\langle \mu_{xx} \rangle = \frac{\mu_{xx}^{1}\mu_{xy}^{2}+f_{a1}f_{b1}[(\mu_{xx}^{1}-\mu_{xx}^{2})^{2}-(\mu_{xy}^{1}-\mu_{xy}^{2})^{2}]}{f_{a1}\mu_{xx}^{2}+f_{b1}\mu_{xx}^{1}} \quad (4.17)$$

$$\langle \mu_{yy} \rangle = \frac{\mu_{xx}^{1}\mu_{xx}^{2}}{f_{a1}\mu_{xx}^{2}+f_{b1}\mu_{xx}^{1}} \quad (4.18)$$

Obtaining the dispersion equation for wave propagation in a material by utilizing the permeability tensor is a straightforward operation.

$$k_y^2(a+b)^2 + k_x^2\left[a^2+b^2-\left[\frac{2\mu_{xy}^{1}\mu_{xy}^{2}}{\mu_{xx}^{1}\mu_{xx}^{2}} - \frac{(\mu_{xx}^{2})^{2}+(\mu_{xy}^{2})^{2}}{\mu_{xx}^{1}\mu_{xx}^{2}} - \frac{(\mu_{xx}^{1})^{2}+(\mu_{xy}^{1})^{2}}{\mu_{xx}^{1}\mu_{xx}^{2}}\right]ab\right] = \frac{\omega^2}{c^2}[(\mu_v^1 a+\mu_v^2 b)(\epsilon_1 a+\epsilon_2 b)] \quad (4.19)$$

The product $[(\mu_v^1 a+\mu_v^2 b)(\epsilon_1 a+\epsilon_2 b)]$ represents the effective medium's response, combining the contributions of the permeabilities and permittivities of the two materials.

The equation (4.19) is a dispersion relation equation that describes the propagation of electromagnetic waves in a superlattice treated as an effective homogeneous anisotropic medium. It shows how the wavevector components $k_x$ and $k_y$ relate to the frequency $\omega$ of the waves, considering the combined effects of the magnetic and electric properties of the materials that make up the superlattice.

## 4.4. DISPERSION RELATION FOR SURFACE MAGNETIC POLARITON IN EFFECTIVE MEDIUM

In this special case, When the second layer is non-magnetic, the effective-medium description of this particular superlattice may be deduced directly from equation (4.16)-(4.18) as $\mu_{xx}^{2} = 1$, and other magnetic contributions are zero$\mu_{xy}^{2} = 0$. the permeability tensor.will be as

$$\langle \mu_{xy} \rangle = \frac{f_{a1}\mu_{xy}^{1}}{f_{a1}+f_{b1}\mu_{xx}^{1}} \quad (4.20)$$

$$\langle \mu_{xx} \rangle = \frac{f_{a1} f_{b1} \left[ (\mu_{xx}^1 - 1)^2 - (\mu_{xy}^1)^2 \right]}{f_{a1} + f_{b1} \mu_{xx}^1} \tag{4.21}$$

$$\langle \mu_{yy} \rangle = \frac{\mu_{xx}^1}{f_{a1} + f_{b1} \mu_{xx}^1} \tag{4.22}$$

The propagation equation for an effective medium, where a nonmagnetic component is present, can be expressed as:

$$k_y^2 (a+b)^2 + k_x^2 [a^2 + b^2 (\mu_v^1 + \frac{1}{\mu_{xx}^1}) ab] = \frac{\omega^2}{c^2} (\mu_v^1 a + b)(\epsilon_1 a + \epsilon_2 b) \tag{4.23}$$

For damping waves $k_y^2 = -\beta^2$ and the expression (4.23) can be rewritten in the following form:

$$\beta^2 = k_x^2 [f_a^2 + f_b^2 + (\mu_v^1 + \frac{1}{\mu_{xx}^1}) f_a f_b] = \frac{\omega^2}{c^2} (\mu_v^1 f_a + f_b)(\epsilon_1 f_a + f_b \epsilon_2) \tag{4.24}$$

In conclusion, the effective-medium theory for magnetic superlattices at long wavelengths is derived in terms of expansion and continuity arguments, giving a general description of the system. By introducing a new Brillouin-zone edge into the superlattice structure, it can be interpreted how the elementary excitation spectrum is modified. This helps the analysis of long-wavelength excitations in the system.

Two magnetic media with gyro tropic permeability tensors are considered by this theory so that the behavior of the system may be understood as an anisotropic bulk medium in the limit of long wavelengths.

# PART 5

# THE EFFECT OF AN EXTERNAL MAGNETIC FIELD ON THE SPECTRA OF MAGNETIC POLARITONS

This chapter is essential for comprehending the manner in which the magnetic characteristics of the system interact with external influences, such as magnetic fields, and how these interactions impact the spectra of polaritons and waves [45].

## 5.1. LOCALIZED MAGNETIC POLARITONS AT THE BOUNDARY

The objective of the study is to investigate the localized magnetic polaritons that arise at the interface between two antiferromagnetic superlattices. The superlattices are connected together by an anti-ferromagnetic layer and exposed to an external magnetic field. The surface-determined localized magnetic polariton modes are obtained by solving Maxwell's equations. while ensuring that the electromagnetic boundary conditions are met at the interface with an anti-ferromagnetic layer.. Within this framework, we apply effective medium theory to describe the behavior of antiferromagnetic superlattice as an anisotropic bulk medium [45].

Numerical studies were undertaken to investigate how the spectrum of surface-guided polaritons changes under influence of an external magnetic field and its relation to the physical characteristics of a contact film in different antiferromagnetic systems. Its technical applications, including waveguide devices, would benefit from this study’s results.

## 5.2. MAGNETIC POLARITONS AND THEIR APPLICATIONS

The magnetic polariton is a well-known phenomenon that serves as a connection between electromagnetic waves (photons) and elementary excitations like magnons. The system comprises both surficial mode and massive bulk magnetopolaritons, which can be excited in ferromagnets, antiferromagnets, magnetic superlattices, and other magnetically ordered media. This coupling leads to an increase in the intensity of electromagnetic fields that is very useful for nanotechnology such as biosensing, waveguide applications of nano-devices, and antennas. Most publications are concerned with surface magnetic polaritons that are sustained by magnetic materials. Thin films can exhibit both surface polaritons, which are confined to the surface, and guided modes, which are defined by standing wave-like excitation within the film[46,47]. The study of these specific electromagnetic modes, known as retarded electromagnetic modes or magnetic polaritons, has been thoroughly examined in many finite systems, primarily focusing on thin film and other planar geometries [35,46].

## 5.3 THEORETICAL AND EXPERIMENTAL BACKGROUND

The most recent research has concentrated on examining the surface magnetic poles in antimagnetic superlattices using both theoretical and experimental methods[48–50]. There is a growing interest in studying spin wave excitations in long magnetic nanowires and nanotubes. This interest is backed by both practical and theoretical research [51,52]. Prior studies have also examined surface and magnetic polaritons in two-dimensional nano slab-aligned multilayer devices [53,54]. Theoretical investigations have extensively examined several antiferromagnetic-based superstructures, analyzing the properties of both bulk and surface excitations in these systems [50,55,56].

Antiferromagnetic superlattices are highly significant in the field of communications and signal processing technologies, particularly for devices that operate at infrared wavelengths[57,58]. The objective of this work is to determine the dispersion relation for magnetic polaritons that arise at the boundary between an antiferromagnetic film and two antiferromagnetic superlattices. The research utilizes the effective-medium

approximation in the Voigt configuration, employing macroscopic theory and taking into account the existence of an external magnetic field.

## 5.4. APPLICATION OF EFFECTIVE-MEDIUM THEORY TO ANTIFERROMAGNETIC SUPERLATTICES

The effective-medium hypothesis is suitable for antiferromagnetic superlattices due to their resonance frequencies being within the far infrared region, and these superlattices displaying features that are typical of an anisotropic bulk medium[46,50,59].

In this framework, the dielectric tensor and permeability tensor components are defined as spatial averages of the dielectric and permeability constants across the individual magnetic layers that compose the superlattice. The study focuses on a system comprising two antiferromagnetic superlattices (SL) with periods $L1 = a1 + b1$ and $L2 = a2 + b2$ connected to a thin antiferromagnetic film with a thickness of $d$.

## 5.5 CALCULATION OF EFFECTIVE-MEDIUM PERMEABILITY

The effective medium is defined by the effective-medium permeability tensor, which may be calculated using its constituent components:

$$\langle \mu_{xx} \rangle = \frac{(a+b)^2 \mu_1^1 \mu_1^2 + ab[(\mu_1^1 - \mu_1^2)^2 - (\mu_2^1 - \mu_2^2)^2]}{(a+b)(a\mu_1^2 + b\mu_1^1)} \tag{5.1}$$

$$\langle \mu_2 \rangle = \frac{a\,\mu_2^1 \mu_1^2 + b\,\mu_2^2 \mu_2^1}{(a+b)(a\mu_1^2 + b\mu_1^1)} \tag{5.2}$$

$$\langle \mu_{yy} \rangle = \frac{(a+b)\,\mu_1^1 \mu_1^2}{a\mu_1^2 + b\mu_1^1} \tag{5.3}$$

### 5.5.1. Dielectric Tensors For Te Mode

The essential dielectric tensor component for the TE mode in the effective-medium description is:

$$\boldsymbol{\varepsilon_{xx}^{SL}} = \frac{\boldsymbol{a\varepsilon_1 + b\varepsilon_2}}{\boldsymbol{a+b}} \tag{5.4}$$

Where $\varepsilon_i (i = 1, 2)$ represents the dielectric constant of the i-th component of the superlattice.

the terms, $\mu_1^i$ and $\mu_2^i$ represent the non-vanishing element of the frequency-dependent magnetic permeability tensor which depends on the frequency we have:

$$\hat{\mu}^i(\omega) = \begin{bmatrix} \mu_1^{(i)} & i\mu_2^{(i)} & 0 \\ -i\mu_2^{(i)} & \mu_1^{(i)} & 0 \\ 0 & 0 & 1 \end{bmatrix} \tag{5.5}$$

and for an antiferromagnet $\hat{\mu}^i(\omega)$ are defined by:

$$\mu_1(\omega) = 1 + \frac{\Omega_a \Omega_m}{\Omega_1^2 + \omega_+^2} + \frac{\Omega_a \Omega_m}{\Omega_1^2 - \omega_-^2} \tag{5.6}$$

$$\mu_2(\omega) = 1 + \frac{\Omega_a \Omega_m}{\Omega_1^2 + \omega_+^2} - \frac{\Omega_a \Omega_m}{\Omega_1^2 - \omega_-^2} \tag{5.7}$$

where $\Omega_a$and $\Omega_m$ are parameters related to the magnetic properties of the superlattice, they are expressed in terms of the magnetization $M_0$and external field $H_0$ :

$\Omega_m = \gamma 4\pi M_0$ and $\Omega_0 = \gamma H_0$

the antiferromagnetic resonance frequency $\Omega_0$ is divided into two different frequencies, denote as $\omega_\pm = \omega \pm \Omega_0$ by the magnetization $M_0$. Antiferromagnetic resonance frequency $\Omega_1$is determined by the anisotropy field $H_{an}$ and exchange field $H_{ex}$ as:

$$\Omega_1 = \gamma[H_{an}(2H_{ex} + H_{an})]^{\frac{1}{2}} \quad (5.8)$$

These expressions define the behavior of the magnetic permeability tensor for the TE mode in an antiferromagnetic system.

## 5.6. DYNAMICS OF THE MAGNETIC FIELD IN MAGNETIC SYSTEMS

In this context, the dynamic magnetic field $\vec{h}(\vec{r}, t)$ obeys the subsequent equation, which is obtained by removing $\vec{E}(\vec{r}, t)$ from the curl equations derived from Maxwell's equations:

$$\nabla^2\vec{h} - \vec{\nabla}(\vec{\nabla}\vec{h}) - \frac{\varepsilon}{c^2}\frac{\partial^2}{\partial t^2}(\vec{h} + 4\pi\vec{m}) = 0 \quad (5.8)$$

This equation governs the behavior of the dynamic magnetic field in the presence of the magnetization field $\vec{m}$ In the context of antiferromagnetic superlattices. It can be expressed in the following form:

For the first superlattice (SL1) where $y < 0$:

$$h^1 = \left(\langle H_x^1\rangle, \langle H_y^1\rangle\right)\mathrm{e}^{\beta_1 y}\mathrm{e}^{\mathrm{i}(kx-\omega t)} \quad (5.9)$$

For the second superlattice (SL2) where $y > 0$:

$$h^2 = \left(\langle H_x^2\rangle, \langle H_y^2\rangle\right)\mathrm{e}^{-\beta_2 y}\mathrm{e}^{\mathrm{i}(kx-\omega t)} \quad (5.10)$$

Concerning the contact film located in the region $0 < y < d$:

$$h^0 = \left[\left(H_{1x}^0, H_{1y}^0\right)e^{\alpha_0 y} + \left(H_{2x}^0, H_{2y}^0\right)e^{-a_0 y}\right]\mathrm{e}^{\mathrm{i}(kx-\omega t)} \quad (5.11)$$

These expressions describe the behavior of the magnetic field components in different regions of the superlattice system. By applying boundary conditions and solving Maxwell's equations, we can determine the specific modes of localized magnetic polaritons. This study facilitates comprehension of the spread and interaction of magnetic polaritons and magnetostatic waves in the presence of an external magnetic field, which is essential for the design and development of advanced waveguide devices and other technological applications.

## 5.7. BOUNDARY CONDITIONS AND DISPERSION RELATION

In the region where the contact film is located, 0 < y < d, the following conditions apply:
we have:

$$\beta_i^2 = -k_y^2 \quad \text{and } \alpha_0^2 = k^2 - \frac{\omega^2}{c^2}\mu_v^j.$$

In this context $\langle H_{x,y}^i \rangle, \langle B_{x,y}^i \rangle$, represent the average values of $H_{x,y}^i$ and $B_{x,y}^i$in the superlattice. The parameter $\alpha_0$ in the final equation might have either a real value (for surface modes) or an imaginary value (for guided modes). In order to guarantee bounded excitation, it is crucial for the wave vector $\beta_i$ to possess both real and positive values. In order to get the dispersion relation for surface-guided magnetic polaritons (SGP), we utilize electromagnetic boundary conditions at the surfaces of the contact film, especially at $y = 0$ and $y = d$. These requirements ensure that the tangential component of the magnetic field vector $\vec{h}$ and the normal component of the vector $\vec{b}$ remain continuous. After conducting many algebraic operations, the following outcome is derived:

$$\frac{1}{A}\Big\{\mu_1^0\,\alpha_0\cos^{(\alpha_0 d)}\Big[\big(k\mu_2^2+\beta_1\mu_{yy}^1\big)\Big(\varepsilon_2\frac{\omega^3}{c^2}\mu_{yy}^2-k^2\Big)-\big(k\mu_2^2-\beta_2\mu_{yy}^2\big)\Big(\varepsilon_1\frac{\omega^2}{c^2}\mu_{yy}^1-k^2\Big)\Big]\sin(\alpha_0 d)\Big[\big(K\mu_2^1+\beta_1\mu_{yy}^1\big)\Big\{k\mu_2^0\Big(\varepsilon_2\frac{\omega^2}{c^2}\mu_{yy}^2-k^2\Big)-\big(k\langle\mu_2^2\rangle-\beta_2\mu_{yy}^2\big)\Big(\varepsilon_0\frac{\omega^2}{c^2}\mu_1^0-k^2\Big)\Big\}+\Big(\varepsilon_1\frac{\omega^2}{c^2}\mu_{yy}^1-k^2\Big)\Big\{k\,\mu_2^0\big(k\,\langle\mu_2^2\rangle-\beta_2\mu_{yy}^2\big)-\mu_v^0\,\mu_1^0\Big(\varepsilon_2\frac{\omega^2}{c^2}\mu_{yy}^2-k^2\Big)\Big\}\Big]\Big\}=0 \tag{5.12}$$

$$A^{-1}=\Big(\varepsilon_1\frac{\omega^2}{c^2}\mu_{yy}^1-k^2\Big)\Big(\varepsilon_2\frac{\omega^2}{c^2}\mu_{yy}^2-k^2\Big)\Big(\varepsilon_0\frac{\omega^2}{c^2}\mu_1^0-k^2\Big) \tag{5.13}$$

The expression is a complicated polynomial equation in terms of $(k)$and $(\omega)$, This defines the dispersion relation for surface-guided polaritons. The roots of this equation will give the possible values of $(k)$ and $(\omega)$ for which these surface-guided polaritons can exist.

The parameter $\beta_i$ represents the decay rate of the magnetic polaritons in the i-th superlattice, indicating the damping along the axis of the SL. Specifically, $\beta_1$ corresponds to the damping when y approaches positive infinity ( $\beta_1$ for $y \to +\infty$), and when y approaches negative infinity ( $\beta_1$ for $y \to -\infty$)

The term $(Re\beta_i)^{-1} > 0$ represents the penetration depth of the magnetic polaritons into the i-th superlattice. The parameter$\beta_i$ may be derived from the dispersion relation for bulk magnetic polaritons in the effective medium.[3]

Where:

$$f_{ai} = \frac{a_i}{a_i+b_i} \ , \ f_{bi} = \frac{b_i}{a_i+b_i}$$

$$\beta_i^2 = k^2\left[f_{a_i}^2 + f_{b_i}^2 + f_{a_i}f_{b_i}\frac{\mu_\nu^{1(i)}\mu_1^{1(i)}+\mu_\nu^{2(i)}\mu_1^{2(i)}+2\,\mu_\nu^{2(i)}\mu_2^{2(i)}}{\mu_1^{1(i)}\mu_1^{2(i)}}\right] - \frac{\omega^2}{c^2}\left(f_{a_i}e_1^i + f_{bi}e_2^i\right)\left(f_{a_i}\mu_{\nu 1}^{1(i)} + f_{bi}\mu_\nu^{2(i)}\right) \quad (5.14)$$

The frequency of the localized magnetic polaritons in a system composed of two semi-infinite antiferromagnetic superlattices connected by an antiferromagnetic film in the effective-medium description are determined by equation (5.13) and equation (5.14). The provided equation represents the overall dispersion relation for surface-localized magnetic polaritons that travel in the same direction as the contact film, perpendicular to the magnetic moments and the external magnetic field (in Voigt geometry). This equation is applicable to both ferromagnetic and antiferromagnetic systems.

Thin contact films exhibit both surface polaritons, which are localized excitations at the surface, and guided modes, which have a standing wave-like nature within the film. Hence, the parameter $\alpha_0$ in equation (12) can now take on either a purely real value (indicating surface modes) or a wholly imaginary value (indicating guided modes). To ensure a bounded excitation, the wave vector $\beta_i$ must be both real and positive.

## 5.8. NUMERICAL CALCULATIONS

We present our analyses for the antiferromagnetic superlattice $SL(MnF2/ZnF2)$ and antiferromagnetic superlattice $SL(2 * MnF2/ZnF2\ )$ with antiferromagnetic contact film $FeF_2$.

Here we assume the thickness of contact film $d = 0.0005cm$. The magnetic polariton spectra can be seen in the subsequent figures, illustrating the decreased frequency.

$\omega^* = \frac{\omega}{\Omega_m^{(MnF2)}}$ against the wavevector $k^* = \frac{ck}{\Omega_m^{(MnF2)}}$.

The various symbols, such as open and solid squares, triangles, and dots, represent the surface (SM) and guided (GM) components. Here, we utilize the subsequent parameters.

for $MnF_2$:

- $M0 = 0.754\ T$,
- $Hex = 55\ T$,
- $H_{an} = 0.787\ $ ,
- $\gamma = 4.5$,
- $\varepsilon = 5{,}5$ ,

and $FeF_2$ :

- $M0 = 0.624\ T$,
- $Hex = 54\ T$,
- $H_{an} = 20\ T$ ,
- $\gamma = 1.05$,
- $\varepsilon = 5{,}5$.

the non -magnetic material has a value of $\varepsilon = 8$.

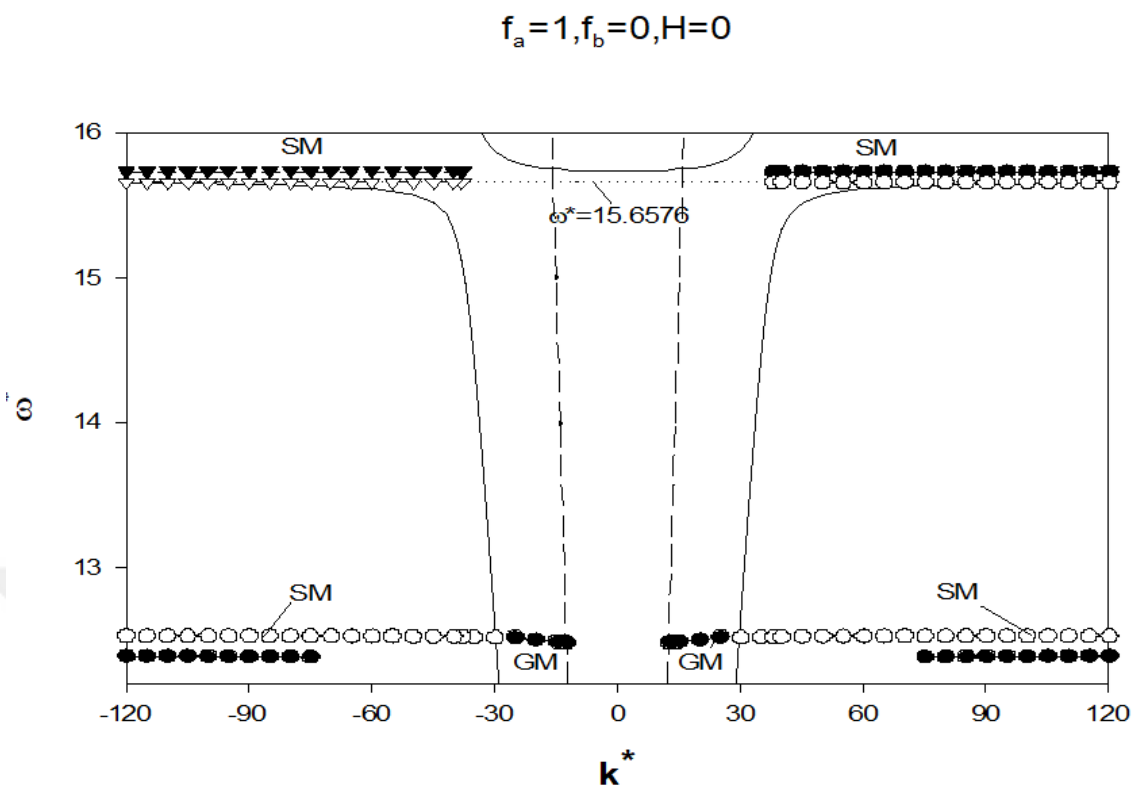


Fig. 5.1. Shows the dispersion relation for surface polaritons and bulk in $FeF_2$ antiferromagnetic film with a magnetic field of zero $H = 0$, $f_a = 1$, $f_b = 0$ [8].

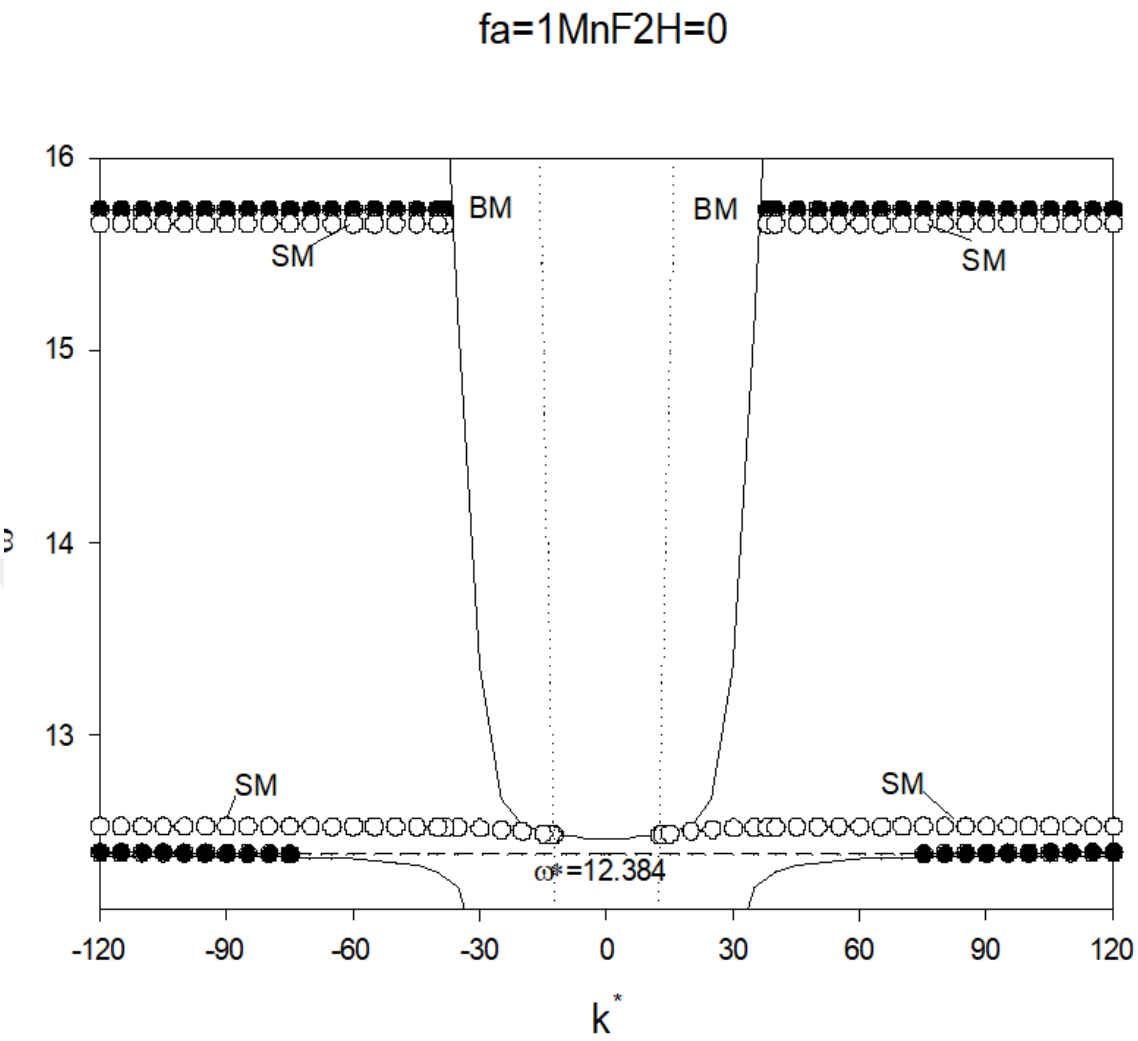


Fig. 5.2. Presents the dispersion relation for bulk and surface (directed) polaritons in a bulk $MnF_2$ antiferromagnetic film with a magnetic field of zero $H = 0$, $f_a$ =1, $f_b = 0$. [8]

The figures (Figs.5.1-5.2) display the findings of the system with two bulk antiferromagnets connected to the antiferromagnetic film, under the conditions $fa = 1$ and $fb = 0$, with no external field applied. When there is no external magnetic field, we see two frequency areas that indicate the collective vibrations of the material and five distinct branches of magnetic polaritons that are confined to the surface or led along it, for each direction of $k^*$. There are two high-frequency surface modes that occur between the bulk bands of $F_eF_2$. These modes start at a finite value of the wavevector and have an antiferromagnetic resonance frequency of $\omega_1^{(F_eF_2)^*} =$ 15,6576in the absence of an external magnetic field, as indicated by Equation (5.8). The low-frequency SM branches, shown in Figure 5.2), begin at the resonance

frequency $\omega_2^{(M_nF_2)^*} = 12.384$ and k=75 and k=75, and approach the frequency $\omega_{m2}^{(M_nF_2)^*} = 12.4261$ . The frequency $\omega_{m2}^{(M_nF_2)}$ represents the magnetostatic frequency in $M_nF_2$, as well as in the semi-infinite antiferromagnet. Aside from the surface modes, there is a single guided mode that branches out from the photon line at $K = 12.5$ ($\omega^* = 12.484$). This guided mode persists within a limited range of $k^*$, but as the absolute value of $|k^*|$increases, it transitions into the surface mode at ($\omega^* = 12.519$). The frequency of the surface (guided) mode is independent of the wave vector's sign, indicating that the surface modes are reciprocal.

# PART 6

# MAGNON POLARITONS AT THE JUNCTION OF TWO ANTIFERROMAGNETIC SUPERLATTICES WITH GRAPHENE AT THE CONTACT INTERFACES

## 6.1 THE PHYSICAL PROPERTIES OF GRAPHENE

It is well recognized that nowadays the focus of the literature is mostly on the physical characteristics of graphene. The study in [60] examined the characteristics of Plasmon modes in monolayer graphene on a substrate. The analysis considered the thickness of both the graphene layer and the substrate material layer when evaluating the Coulomb potential. The study demonstrated that the plasmon mode in monolayer graphene exhibits a linear dispersion, unlike multilayer graphene, particularly in the long-wavelength limit. The gradient of the plasmon spectrum is dictated by the substrate's thickness and dielectric constant.

In a study done with[61], the impact of electron density on the electron-phonon interaction and Coulomb pseudopotential in graphene was analyzed. Additionally, the factor of isotopic shifting in a graphene monolayer on a substrate was determined.

Polaritons in quasi-2D materials may be excited throughout a wide range of the electromagnetic spectrum, spanning from microwave to ultraviolet wavelengths. Within this extensive range, notable research has been conducted on the elementary excitations in structures that incorporate a graphene layer at the material interfaces. The presence of graphene is crucial in generating unique polariton properties[16,62], facilitating the

propagation of light waves[63], and influencing the thermal properties of multilayered systems [64]. Specifically, when examining a stacked arrangement consisting of graphene and an insulating antiferromagnet, with a dielectric layer separating them that is approximately 500 nm thick, there are additional phenomena to consider. These include the interaction between antiferromagnetic surface polariton modes and the plasmon-polariton of the graphene sheet [65]. This research discovered the presence of two distinct forms of polariton modes: a surface magnon plasmon polariton, which occurs at specific carrier densities in graphene, and a surface plasmon magnon polariton, which is created by the interaction between the graphene surface plasmon and the antiferromagnetic magnon mode. This research has the potential to generate distinct characteristics of these collective forms. In this study, we focus on examining the transmission of magnon-polaritons in a gyromagnetic system. The system consists of a graphene sheet positioned at the boundary of two infinite media. One of these media can be either ferromagnetic or antiferromagnetic, while the other is nonmagnetic. The user's text is [14].

## 6.2. THE JUNCTION OF TWO ANTIFERROMAGNETIC SUPERLATTICES WITH GRAPHENE AT THE CONTACT INTERFACES

### 6.2.1. Dispersion Relation For Surface Magnetic Polaritons At The Junction Of Two Antiferromagnetic Superlattices With Graphene At The Contact Interfaces

The aim of our study is to investigate the behavior of surface magnon-polaritons – quasiparticles that result from the interaction between magnons (spin waves) and photons at the interface of two antiferromagnetic superlattices separated by an antiferromagnetic slab with graphene layers at the interfaces. The present research mainly deals with how changing the Fermi energy in graphene, through different electronic doping levels, can affect the spectrum of surface magnon-polariton modes and to investigate the mode localization effects.

It is essentially that although graphene itself is neither ferromagnetic nor antiferromagnetic, that it may have a strong influence on the magnetic modes (e.g.), on their dispersion and reciprocal/nonreciprocal propagation properties). The Fermi energies in the graphene can be varied by employing different electronic doping levels, resulting in a strong influence exerted by the presence of graphene on the surface magnon-polariton modes. Fermi energies in graphene can be varied using different levels of electronic doping. This is caused by a strong effect exerted on the surface magnon-polariton modes of graphene surfaces. These effects include localization of modes and control of group velocities of modes as the Fermi energies of graphene sheets change, as well as an important role of phenomenological damping in graphene sheets.

Firstly, we describe the system under consideration. As one can see from **Fig. 6.1**

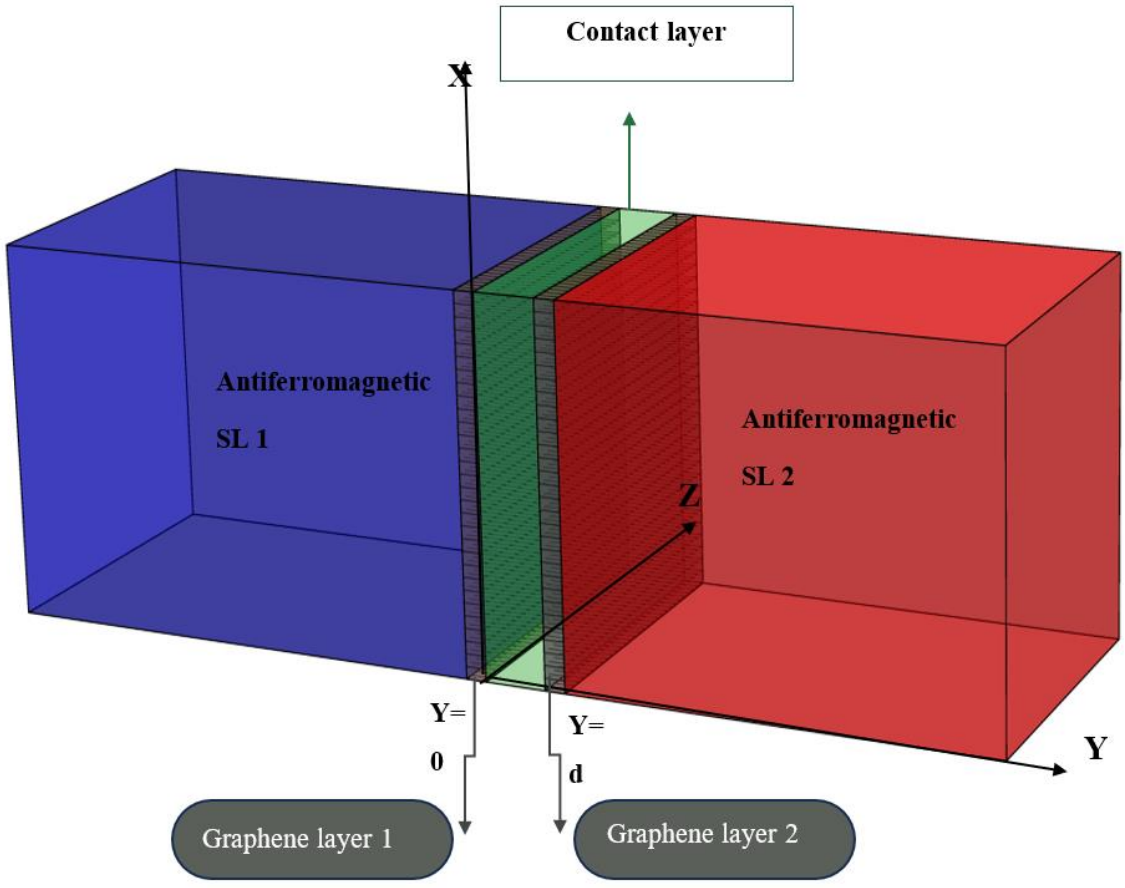


Fig. 6.1. Two Antiferromagnetic Superlattices Separated by a Contact Layer with Graphene Layers at Interfaces

The superstructure is composed of two antiferromagnetic superlattices(antiferromagnetic materials and nonmagnetic spacers), with a defined

geometry and coordinate axes. divided by the contact slab filling the region 0<y<d. At the planar interfaces y=0 and y=d, there is a 2D graphene sheet present. In this case, we examine a system consisting of two antiferromagnetic superlattices (SL) with the corresponding periods $L1 = a1 + b1$ and $L2 = a2 + b2$. These superlattices are also connected to a thin antiferromagnetic film with a thickness of d. The variables $a_i, b_i (i = 1,2)$ represent the thickness of the superlattice components, respectively. A static magnetic field, denoted as $\mathbf{H_0}$, is provided parallel to the interface and aligned with the z-axis, which is also parallel to the static magnetization, denoted as $\mathbf{M_0}$, in the gyromagnetic medium. The computations are performed for the propagation wave vector **k** in the ±**x** directions (Voigt geometry).

When a static magnetic field is applied parallel to the 2D graphene sheet, the electrical conductivity of the graphene sheet at optical frequencies remains unaltered. This is in contrast to the effect of a perpendicular applied field. The selection of conductivity is based on the random-phase approximation and may be accurately characterized for low frequencies and extensively doped graphene using the Drude-like formula [66], which is as follows:

$$\sigma = \frac{4\pi i e^2 E_F}{\hbar(\omega + iG)}$$

In this context, e represents the electronic charge, Planck's constant is denoted as $\hbar$, $E_F$ Standsfor the Fermi energy, ω is the angular frequency, and G is the phenomenological damping associated with electron scattering. Surface magnetic polaritons are exclusively present in the situation of s-polarization, namely for transverse electric (TE) modes, due to the realisation of mode localization [12].

The calculation of surface magnon-polariton modes entails solving Maxwell's electromagnetic equations separately in each of the three regions (Superlattice 1, contact layer, and Superlattice 2) and implementing electromagnetic boundary conditions at the interfaces, where the graphene layers are situated.

At the long-wavelength limit, the antiferromagnetic superlattice exhibits similar behavior to an anisotropic bulk medium, allowing us to utilize the effective-medium approximation.

The electric field in medium 1 (antiferromagnetic Superlattice 1) and medium 3 (antiferromagnetic Superlattice 2) for the TE- modes may be expressed as:

$$<\text{Ez}>^{(SL1)} = <\text{Az}>^{(1)} e^{\beta 1 y}\, e^{i(kx-\omega t)}, y < 0; \quad (6.1)$$

$$<\text{Ez}>^{(SL2)} = <\text{Az}>^{(SL2)} e^{-\beta 2 y}\, e^{i(kx-\omega t)},\ y > d; \quad (6.2)$$

For the contact layer in ( 0<y<d):

$$Ez^{(0)} = (A\, e^{\alpha 0 y} + C e^{-\alpha 0 y}) e^{i(kx-\omega t)} \quad (6.3)$$

By applying Ampere's law, we may express the magnetic field components in each medium. Next, by utilizing the Ampere's law:

$$\vec{B} = (1/i\omega)\vec{\nabla} \times \vec{E}; \quad (6.4)$$

we can convey the magnetic field components in each medium using the following format:
for SL1:

$$<\vec{B}>^{(SL1)} = [(1/\text{i}\omega)(\beta_1 \vec{x} - \text{ik}\vec{y})] <\text{Ez}>^{(Sl1)} \quad (6.5)$$

for SL2:

$$<\vec{B}>^{(SL2)} = [(-1/\text{i}\omega)(\beta_2 \vec{x} + \text{ik}\vec{y})] <\text{Ez}>^{(Sl2)} \quad (6.6)$$

For the magnetic slab:

$$\vec{B}^{(0)} = -i\,(A\, e^{\alpha 0 y} - C e^{-\alpha 0 y}) e^{i(kx-\omega t)} \quad (6.7)$$

for the magnetic fields components $H$ in each medium obtained from the equation $B = \tilde{\mu}\vec{H}$

So after some algebra the equations (6.5) (6.7) can be written as the follows:

$$\langle H_x^{SL1}\rangle = \frac{1}{i\omega\langle\mu_v^1\rangle}\left[\beta_1\,\langle\mu_{yy}^{(1)}\rangle - \langle\mu_{xy}^{(1)}\rangle k\right]\langle E_z^{SL1}\rangle \tag{6.8}$$

$$\left\langle H_y^{SL1}\right\rangle = \frac{1}{i\omega\langle\mu_v^1\rangle}\left[i\beta_1\,\langle\mu_{xy}^{(1)}\rangle - ik\langle\mu_{xx}^{(1)}\rangle\right]\langle E_z^{SL1}\rangle \tag{6.9}$$

For the contact layer

$$H_x^0 = -\frac{1}{\mu_0'\omega}[\Lambda_- - Ae^{\alpha_0 y} + \Lambda_+ ce^{-\alpha_0 y}]e^{i(kx-\omega t)} \tag{6.10}$$

Where : $\Lambda_\pm = i\left(\mp\alpha_0\mu_{yy}^{(0)} - \mu_{xy}^{(0)}k\right)$

$$\langle H_x^{SL2}\rangle = \frac{1}{i\omega\langle\mu_v^2\rangle}\left[-\beta_2\,\langle\mu_{yy}^{(2)}\rangle - \langle\mu_{xy}^{(2)}\rangle k\right]\langle E_z^{SL2}\rangle \tag{6.11}$$

$$\left\langle H_y^{SL2}\right\rangle = \frac{1}{i\omega\langle\mu_v^2\rangle}\left[-i\beta_2\,\langle\mu_{xy}^{(2)}\rangle - ik\langle\mu_{xx}^{(2)}\rangle\right]\langle E_z^{SL2}\rangle$$

Here $\langle\mu_v^i\rangle = \langle\mu_{xx}^{(i)}\rangle\langle\mu_{yy}^{(i)}\rangle - \langle\mu_{xy}^{(i)}\rangle^2$,

(i- SL's number) and

$$\mu_0' = \left(\mu_{xy}^{(0)}\right)^2 - \mu_{xx}^{(0)}\mu_{yy}^{(0)} \tag{6.12}$$

Using the electromagnetic boundary conditions at the interfaces located at y=0 and y=d in the presence of graphene,

we have:

$<Ez>^{(SL1)}\rfloor_{y=0} = Ez^{(0)}\rfloor_{y=0}$; (6.13)

$(H_x{}^{(0)} - <H_x{}^{Sl1}>)\big|y = 0 = \vec{J} = \sigma^{(1)}Ez^{(0)}$, for y=0 (6.14)

$Ez^{(0)}\rfloor_{y=d} = <Ez^{(SL2)}>\rfloor_{y=d}$ (6.15)

$(<Hx^{Sl2}> - Hx^{(0)})\big|y = d = \sigma^{(2)}\langle Ez\rangle^{(Sl2)}$, for y=d. (6.16)

Here j-electric current density , $\sigma^{(i)}$is the conductivity for a graphene sheet for low frequencies can be written using a Drude –like formula :

$$\sigma \approx \frac{ie_0 c 8\pi E_F}{137h(\omega+iG)} \quad (6.17)$$

Where $E_F$ is Fermi enerji, G represents the phenomenological damping related to electron,

$\beta_i (i = 1,2)$ represents the decay constant and $(Re\beta_i)^{-1} > 0$ denotes the penetration depth of the polaritons into the i-superlattice. By applying algebraic techniques, we can express the dispersion relation for the surface magnon-polariton modes. These modes propagate specifically at the junction where two antiferromagnetic superlattices meet, with graphene present at the contact surfaces.

$$e^{-2\alpha_0 d} = \frac{(P1+i\frac{\omega}{c}\sigma'^{(1)}+i\frac{L_+}{\mu_v^{(o)}})(P2+i\frac{\omega}{c}\sigma'^{(2)}-i\frac{L_-}{\mu_v^{(o)}})}{(P1+i\frac{\omega}{c}\sigma'^{(1)}+i\frac{L_-}{\mu_v^{(o)}})(P2+i\frac{\omega}{c}\sigma'^{(2)}-i\frac{L_+}{\mu_v^{(o)}})} \quad (6.18)$$

Where: $\sigma'^{(i)} = \frac{\sigma^{(i)}}{c\varepsilon_0}$, i=1,2; c-vacuum light speed, and $\varepsilon_0\mu_0 = \frac{1}{c^2}$

$P1 = (\beta_1 \langle\mu_{\mu_{yy}}^{(1)}\rangle - k \langle\mu_{\mu_{xy}}^{(1)}\rangle)/ \langle\mu_{\mu_v}^{(1)}\rangle$ ;

$P2 = (\beta_2 \langle\mu_{\mu_{yy}}^{(2)}\rangle + k \langle\mu_{\mu_{xy}}^{(2)}\rangle)/ \langle\mu_{\mu_v}^{(2)}\rangle$ ;

$L_+ = -i\,\alpha_0 \langle\mu_{\mu_{yy}}^{(0)}\rangle - i\,k\,\mu_{\mu_{xy}}^{(0)}$;

$$L_{-} = i\,\alpha_0 \langle \mu_{\mu_{yy}^{(0)}} \rangle - ik\, \mu_{\mu_{xy}^{(0)}} \quad (6.19)$$

The decay constant of the i-th superlattice, denoted as $\beta_i (i = 1,2)$, is calculated using the formulae (4.19-4.24) as explained in Part 4.

By considering equation (6.19) while solving equation (6.18), we can determine the frequencies of the localized surface magnetic polaritons. These polaritons propagate at the junction of two antiferromagnetic superlattices, separated by the antiferromagnet slab with the graphene layer on the interfaces. I n the limit $\langle \mu_{yy}^{(1)} \rangle = 1$ and $\langle \mu_{xy}^{(1)} \rangle$=0 , $\langle \mu_{yy}^{(2)} \rangle = 1$ and $\langle \mu_{xy}^{(2)} \rangle$=0 he equation (6.18) is converted into the dispersion relation for surface magnetic polaritons in the gyromagnetic slab with graphene sheets at the interfaces, as discussed in the previous study[14].

## 6.3. NUMERICAL CALCULATIONS

For numerical calculations antiferromagnetic superlattice $SL(MnF2/ZnF2)$ and antiferromagnetic superlattice $SL(2 * MnF2/ZnF2$ ) with antiferromagnetic contact film $FeF_2$ are used. Here we assume the thickness of contact film $d = 0.0005\ cm$. As well as in Part 5, in the following figures we present the magnetic polariton spectra through a plot of the reduced frequency $\omega^* = \frac{\omega}{\Omega_m^{(MnF2)}}$ against the wavevector $k^* = \frac{ck}{\Omega_m^{(MnF2)}}$. The different symbols (open and solid squares, triangles, dots) denote the surface (SM) corresponding various value of Fermi Energy. The following parameters <u>for $MnF_2$</u> are used:

- $M0 = 0.754\ T$,
- $Hex = 55\ T$,
- $H_{an} = 0.787$ ,
- $\gamma = 4.5$,
- $\varepsilon = 5{,}5$ ,

<u>and $FeF_2$</u> :

- $sM0 = 0.624\ T$,

- $Hex = 54\,T$,
- $H_{an} = 20\,T$ ,
- $\gamma = 1.05$,
- $\varepsilon = 5{,}5$.

For the non -magnetic material we have $\varepsilon = 8$.

Fig 6.2 displays the outcomes of the numerical computations. Regarding the calculations, we have made some assumptions. The conductivity in equation (6.17) for a graphene sheet may be restated as follows:

$$\sigma \approx \frac{ie_0 c 8\pi E_F}{137\hbar(\omega + iG)}$$

We apply the concept of the fine structure constant to express $e2/(2\varepsilon_0 hc) \approx 1/137$. We select $E_F = 0.5\,eV$ (or about $\omega_F/2\pi \approx 121\,THz$ for the Fermi frequency) and $\Gamma/2\pi = 0.318\,THz$ s mentioned in reference [15]. It is seen that the values of the parameters $\omega_m$ and $\omega_0$for the magnetic material are consistently much lower than $\omega_F$, his condition is necessary for the use of equation (6.17) to calculate the conductivity of graphene. It is important to mention that we do not consider the influence of the local magnetic field produced by the electric current on the surface of the graphene sheet.

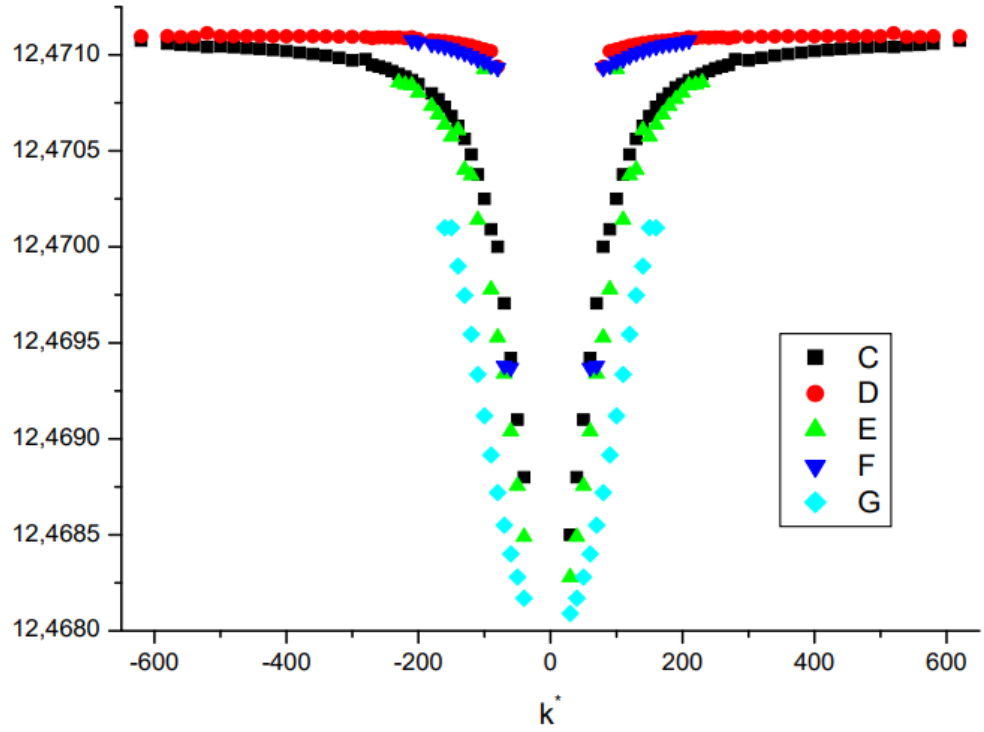


Fig. 6.2. Dispersion relation for surface magnetic polariton modes at the junction of two antiferromagnetic superlattices with graphene at the contact interfaces $H = 0$

Fig6.2. displays the dispersion curves of the surface magnon-polaritons for three different cases. (a) The arrangement consists of graphene at both interfaces in an asymmetric manner, with $E_F^{(1)}$ =0.1eV and $E_F^{(2)}$ = 0.5 eV. This arrangement is represented by red points for high-frequency modes and solid black points for lower-frequency modes. (b) Both interfaces have a graphene sheet with the same doping level, which corresponds to $E_F^{(1)} = E_F^{(2)} = 0.5$ eV. This is indicated by the navy blue and green lines. (c) Both interfaces have a graphene sheet with $E_F^{(1)}$ =1eV and $E_F^{(2)}$ = 1eV, represented by the blue points. The correlation between the $E_F$ values and the conductivity of the graphene sheet(s) remains consistent with earlier assumptions.

In the absence of graphene layers, when $E_F^{(1)}$ =0.eV and $E_F^{(2)}$ = 0. e, a comparable result is seen. In this situation, there are two surface modes for both positive and negative values of k: high-frequency modes and low-frequency modes. It is evident that the curves exhibit symmetry with respect to positive and negative k-wavevectors. Additionally, there are two unique modes present in each example, characterized by

lower and higher frequencies, which may be attributed to the presence of two interfaces.

In Part 5, it was demonstrated that when graphene layers are not present, the low-frequency SM branches begin at the resonance frequency $\omega_m^{(M_nF2)*} = 12.384$ and k*=75 and approach to $\omega_{m_2}^{(M_nF2)*} = 12.4261$, here $\omega_{m_2}^{(M_nF2)}$ represents the magnetostatic frequency in $MnF_2$, as well as in the semi-infinite antiferromagnet. Doping graphene at the interfaces results in a notable upward shift for the pair of modes. These modes are present within a specific and limited range of frequencies, denoted as $\omega * = 12.468 - 12.4711$.

The gap between lower- and higher-frequency modes normally decreases as the wavevector k increases. We have also shown that all curves converge to a common value when k approaches positive or negative infinity. Figure 6.2 demonstrates that the group velocity of the surface lower frequencies modes is significantly greater than the group velocity of the surface higher frequencies modes, as shown by the slope of the curves. Graphene can manipulate the localization and group velocities of magnon-polaritons. This manipulation results in the emergence of both surface and bulk modes in the magnetic heterostructure being studied. The manipulation is achieved by controlling the Fermi energies. Therefore, this necessitates the presence of a certain characteristic in future spintronic devices that employ magnon-polaritons as a way of storing or processing information.

## PART 7

## SUMMARY

The purpose of the present thesis is to investigate the influence of Graphene's presence on the magnon polariton spectrum in(superlattices) magnetic superlattices based on Maxwell's electromagnetic theory. Indeed, graphene exhibits unique features such as high thermal conductivity, exceptional electron transport capabilities, and remarkable mechanical strength, which enable it to form surface magnon-polariton modes at its interface with gyromagnetic media. These modes eventuate in confinement and dispersion of magnon-polaritons.

The study explores incorporating graphene monolayers into magnetic superlattices involving alternating nanoscale materials to examine their electronic, optical, and magnetic properties. The main discovery was that the Fermi energies in graphene allow for bulk and surface modes of magnon polaritons within ferromagnetic crystals by either regulating their localization or group velocities. This regulation has critical implications for devising different spintronic devices that use the magnon-polaritons for information storage and processing.

This study builds upon existing theoretical frameworks and computational models to construct dispersion equations for both bulk and surface magnetostatic modes in layered superlattices. These equations explain how magnetic polaritons behave in structures made from ferromagnetic, antiferromagnetic, or non-magnetic materials. The inclusion of Graphene notably improves the functional properties of these systems.

Additionally, this thesis investigates how external magnetic fields affect the spectra of magnetic polaritons and magnetostatic waves.. As a result, this research helps to gain more insight into electromagnetic interaction in nanoscale magnetic structures thus leading to new directions in materials science and spintronics.

## REFERENCES


1. Pasachoff, N., "The history of electromagnetic theory through the lives of its founders: Nancy Forbes and Basil Mahon: Faraday, Maxwell, and the electromagnetic field: How two men revolutionized physics. Amherst, NY: Prometheus Books, 2014, 320pp, US $25.95 HB", ***Metascience***, 24 (2): 233–236 (2015).

2. Pérez Ramos, T., Romero Blanco, L., Nuñez De Los Santos, I. A., and Peralta Diaz, G., "El legado científico de James Clerk Maxwell: una síntesis", ***Ibero-American Journal Of Engineering & Technology Studies***, 2 (1): 1–8 (2022).

3. Yiğit, E., "Basic Electromagnetic Theory: Electromagnetism", Atmospheric and Space Sciences: Ionospheres and Plasma Environments, ***Springer International Publishing***, Cham, 21–40 (2018).

4. Jens U, N., "Maxwell's equations as mechanical law", ***European Journal Of Physics***, 43 (4): 045202 (2022).

5. Stankovich, S., Dikin, D. A., Dommett, G. H. B., Kohlhaas, K. M., Zimney, E. J., Stach, E. A., Piner, R. D., Nguyen, S. T., and Ruoff, R. S., "Graphene-based composite materials", ***Nature***, 442 (7100): 282–286 (2006).

6. Ferrari, A. C., Meyer, J. C., Scardaci, V., Casiraghi, C., Lazzeri, M., Mauri, F., Piscanec, S., Jiang, D., Novoselov, K. S., Roth, S., and Geim, A. K., "Raman Spectrum of Graphene and Graphene Layers", ***Physical Review Letters***, 97 (18): 187401 (2006).

7. Bludov, Y. V., Gomes, J. N., Farias, G. A., Fernández-Rossier, J., Vasilevskiy, M. I., and Peres, N. M. R., "Hybrid plasmon-magnon polaritons in graphene-antiferromagnet heterostructures", ***2D Materials***, 6 (4): 045003 (2019).

8. Askerbeyli, R. T., "The Influence of External Magnetic Field on the Spectra of Magnetic Polaritons and Magnetostatic Waves", ***Journal Of Superconductivity And Novel Magnetism***, 30 (4): 1115–1122 (2017).

9. Bai, M., Liu, X., Sasaki, T., and Ma, R., "Superlattice films of semiconducting oxide and rare-earth hydroxide nanosheets for tunable and efficient photoluminescent energy transfer", ***Nanoscale***, 13 (8): 4551–4561 (2021).

10. Santos, P. J., Gabrys, P. A., Zornberg, L. Z., Lee, M. S., and Macfarlane, R. J., "Macroscopic materials assembled from nanoparticle superlattices", ***Nature***, 591 (7851): 586–591 (2021).
11. Grishunin, K., Huisman, T., Li, G., Mishina, E., Rasing, T., Kimel, A. V., Zhang, K., Jin, Z., Cao, S., Ren, W., Ma, G.-H., and Mikhaylovskiy, R. V., "Terahertz Magnon-Polaritons in TmFeO $_3$", ***ACS Photonics***, 5 (4): 1375–1380 (2018).
12. Vasconcelos, M. S. and Cottam, M. G., "Magnon-polaritons in ferromagnetic magnonic crystals with graphene at the interfaces", ***Journal Of Physics: Condensed Matter***, 33 (31): 315802 (2021).
13. Liao, L., Puebla, J., Yamamoto, K., Kim, J., Maekawa, S., Hwang, Y., Ba, Y., and Otani, Y., "Valley-Selective Phonon-Magnon Scattering in Magnetoelastic Superlattices", ***Physical Review Letters***, 131 (17): 176701 (2023).
14. Vasconcelos, M. S., Cottam, M. G., and Anselmo, D. H. A. L., "Magnon-polaritons in graphene/gyromagnetic slab heterostructures", ***Journal Of Physics: Condensed Matter***, 33 (5): 055801 (2021).
15. Ta, J.-X., Song, Y.-L., and Wang, X.-Z., "Optical properties of antiferromagnetic/ion-crystal superlattices", ***Journal Of Magnetism And Magnetic Materials***, 324 (1): 72–77 (2012).
16. Tagiyeva, R. T. and Tanatar, B., "Magnetic Polaritons, Magnetostatic Waves and Effective-Medium Approximation for Antiferromagnetic Superlattice with Impurity in Parallel Magnetic Field", ***Journal Of Superconductivity And Novel Magnetism***, 25 (8): 2577–2583 (2012).
17. Ignatchenko, V. A. and Tsikalov, D. S., "Spin Waves in Multilayers with Different Magnitudes of the Magnetization, Exchange, and Anisotropy", ***Solid State Phenomena***, 190: 71–74 (2012).
18. Wapler, M. C., Leupold, J., Dragonu, I., Von Elverfeld, D., Zaitsev, M., and Wallrabe, U., "Magnetic properties of materials for MR engineering, micro-MR and beyond", ***Journal Of Magnetic Resonance***, 242: 233–242 (2014).
19. Stadelmaier, H. H., "Magnetic properties of materials", ***Materials Science And Engineering A***, (2000).
20. Clegg, A., Beckley, P., Snelling, E., and Major, R., "Magnetic Materials", Electrical Engineer's Reference Book, ***Elsevier***, 8-1-8–17 (2003).
21. Surkov, V. V. and Mozgov, K. S., "Effects of the Action of Particle Fluxes and Geomagnetic Variations on Low-Orbital Spherical Satellites", ***Cosmic Research***, 57 (4): 252–260 (2019).

22. Sizov, R. A., "Magnetic and Electric Charges in Physics and Technology of Electromagnetic and Magnetoelectric Induction", ***Journal Of Modern Physics***, 08 (06): 964–981 (2017).

23. Dodonov, V. V. and Dodonov, A. V., "Giant diamagnetism of a quantum charged particle after inversion of the magnetic field", ***Physical Review A***, 105 (6): 062201 (2022).

24. Boyer, T. H., "Diamagnetism of a free particle in classical electron theory with classical electromagnetic zero-point radiation", ***Physical Review A***, 21 (1): 66–72 (1980).

25. Khalid, M., Setzer, A., Ziese, M., Esquinazi, P., Spemann, D., Pöppl, A., and Goering, E., "Ubiquity of ferromagnetic signals in common diamagnetic oxide crystals", ***Physical Review B***, 81 (21): 214414 (2010).

26. Bobkova, I. V., Bobkov, A. M., and Silaev, M. A., "Magnetoelectric effects in Josephson junctions", ***Journal Of Physics: Condensed Matter***, 34 (35): 353001 (2022).

27. Jin, Q., Zhang, Q., Bai, H., Yang, M., Ga, Y., Chen, S., Hong, H., Cui, T., Rong, D., Lin, T., Wang, J.-O., Ge, C., Wang, C., Cao, Y., Gu, L., Song, G., Wang, S., Jiang, K., Cheng, Z.-G., Zhu, T., Yang, H., Jin, K., and Guo, E.-J., "Syntropic spin alignment at the interface between ferromagnetic and superconducting nitrides", ***National Science Review***, 11 (8): nwae107 (2024).

28. Mørup, S., Hansen, M. F., and Frandsen, C., "Magnetic interactions between nanoparticles", ***Beilstein Journal Of Nanotechnology***, 1: 182–190 (2010).

29. Baratchart, L., Chevillard, S., Leblond, J., Lima, E. A., and Ponomarev, D., "Asymptotic method for estimating magnetic moments from field measurements on a planar grid", .

30. Chikurov, D. S. and Volkov, M. P., "Similarity of magnetization and magnetic flux jumps evolution with the magnetic field direction relative to the plane of the superconducting niobium plate", ***Physica C: Superconductivity And Its Applications***, 608: 1354240 (2023).
31. Ahmad, S. I., "Nano cobalt ferrites: Doping, Structural, Low-temperature, and room temperature magnetic and dielectric properties – A comprehensive review", ***Journal Of Magnetism And Magnetic Materials***, 562: 169840 (2022).

32. Rasaili, P., Sharma, N. K., and Bhattarai, A., "Comparison of Ferromagnetic Materials: Past Work, Recent Trends, and Applications", ***Condensed Matter***, 7 (1): 12 (2022).

33. Noori, M. and Altabey, W. A., "Hysteresis in Engineering Systems", ***Applied Sciences***, 12 (19): 9428 (2022).

34. Barnas, J., "Spin waves in superlattices. II. Magnetostatic modes in the Voigt configuration", ***Journal Of Physics C: Solid State Physics***, 21 (22): 4097–4112 (1988).

35. Tagiyeva, R. T., Saglam, M., and Boyacioglu, B., "Dispersion relation for surface-localized magnetic polaritons and magnetostatic waves in antiferromagnetic superlattice", ***Journal Of Physics And Chemistry Of Solids***, 68 (7): 1296–1304 (2007).

36. "Jan, Najser. (2023). Superlattice Dislocations and Magnetic Properties. Doi: 10.1201/9780429070914-120", .

37. Liu, S., Yang, K., Liu, W., Zhang, E., Li, Z., Zhang, X., Liao, Z., Zhang, W., Sun, J., Yang, Y., Gao, H., Huang, C., Ai, L., Wong, P. K. J., Wee, A. T. S., N'Diaye, A. T., Morton, S. A., Kou, X., Zou, J., Xu, Y., Wu, H., and Xiu, F., "Two-dimensional ferromagnetic superlattices", ***National Science Review***, 7 (4): 745–754 (2020).

38. Kumar, S., Mondal, C., and Pathak, B., "Double-Exchange Magnetic Interactions in High-Temperature Ferromagnetic Iron Chalcogenide Monolayers", ***ChemPhysChem***, 20 (6): 873–880 (2019).

39. Bai, H., Zhang, Y. C., Han, L., Zhou, Y. J., Pan, F., and Song, C., "Antiferromagnetism: An efficient and controllable spin source", ***Applied Physics Reviews***, 9 (4): 041316 (2022).

40. (Tagiyeva), R. T. A. and Tanatar, B., "Localized magnetic polaritons in antiferromagnetic superlattice with impurity", ***Journal Of Physics: Conference Series***, 153: 012042 (2009).

41. Li, P., Chen, J., Du, R., and Wang, X.-P., "Numerical methods for antiferromagnetics", ***IEEE Transactions On Magnetics***, 56 (4): 1–9 (2020).

42. Rinkevich, A. B., Milyaev, M. A., and Romashev, L. N., "Ferromagnetic Resonance and Interlayer Exchange Coupling in (Fe/Cr)n Superlattices", ***Physics Of Metals And Metallography***, 120 (3): 247–253 (2019).

43. Tanaka, A., "Ferromagnetism in the Hubbard Model with a Gapless Nearly-Flat Band", ***Journal Of Statistical Physics***, 170 (2): 399–420 (2018).

44. Raj, N. and Tilley, D. R., "Polariton and effective-medium theory of magnetic superlattices", ***Physical Review B***, 36 (13): 7003–7007 (1987).

45. Askerbeyli, R. T., "The Influence of External Magnetic Field on the Spectra of Magnetic Polaritons and Magnetostatic Waves", ***Journal Of Superconductivity And Novel Magnetism***, 30 (4): 1115–1122 (2017).

46. Elmzughi, F. G., Constantinou, N. C., and Tilley, D. R., "Theory of electromagnetic modes of a magnetic superlattice in a transverse magnetic field: An effective-medium approach", ***Physical Review B***, 51 (17): 11515–11520 (1995).

47. Abraha, K. and Tilley, D. R., "Theory of far infrared properties of magnetic surfaces, films and superlattices", ***Surface Science Reports***, 24 (5–6): 129–222 (1996).

48. Karadamoglou, J. and Papanicolaou, N., "Bulk and surface spin-flop transitions in an antiferromagnetic XYZ chain", ***Physical Review B***, 60 (13): 9477–9488 (1999).

49. Schuller, I. K., Kim, S., and Leighton, C., "Magnetic superlattices and multilayers", ***Journal Of Magnetism And Magnetic Materials***, 200 (1–3): 571–582 (1999).

50. Barbillon, G., "Plasmonics and its Applications", ***Materials***, 12 (9): 1502 (2019).

51. Wang, Z. K., Lim, H. S., Liu, H. Y., Ng, S. C., Kuok, M. H., Tay, L. L., Lockwood, D. J., Cottam, M. G., Hobbs, K. L., Larson, P. R., Keay, J. C., Lian, G. D., and Johnson, M. B., "Spin Waves in Nickel Nanorings of Large Aspect Ratio", ***Physical Review Letters***, 94 (13): 137208 (2005).

52. Das, T. K. and Cottam, M. G., "Surface magnetic polaritons in ferromagnetic and antiferromagnetic cylindrical tubes", ***Journal Of Applied Physics***, 103 (7): 07B104 (2008).
53. Zhang, Z., Park, K., and Lee, B. J., "Surface and magnetic polaritons on two-dimensional nanoslab-aligned multilayer structure", ***Optics Express***, 19 (17): 16375 (2011).

54. Zhao, B. and Zhang, Z. M., "Study of magnetic polaritons in deep gratings for thermal emission control", ***Journal Of Quantitative Spectroscopy And Radiative Transfer***, 135: 81–89 (2014).

55. Stamps, R. L. and Camley, R. E., "Green's functions for antiferromagnetic polaritons. I. Surface modes and resonances", ***Physical Review B***, 40 (1): 596–608 (1989).

56. Guimarães, E. S. and Albuquerque, E. L., "Spin canted magnetic polaritons in thin films", ***Solid State Communications***, 122 (11): 623–628 (2002).

57. Brown, D. E., Dumelow, T., Parker, T. J., Abraha, K., and Tilley, D. R., "Nonreciprocal reflection by magnons in FeF 2 : A high-resolution study", ***Physical Review B***, 49 (17): 12266–12269 (1994).

58. Abraha, K., Brown, D. E., Dumelow, T., Parker, T. J., and Tilley, D. R., "Oblique-incidence far-infrared reflectivity study of the uniaxial antiferromagnet FeF 2", ***Physical Review B***, 50 (10): 6808–6816 (1994).

59. Elmzughi, F. G. and Camley, R. E., "Theory of electromagnetic modes of magnetic effective-medium films", ***Journal Of Physics: Condensed Matter***, 9 (5): 1039–1048 (1997).

60. Askerzade, I. N. and Askerbeyli, R. T., "Plasmon spectrum of graphene monolayer on substrate", ***Modern Physics Letters B***, 33 (09): 1950102 (2019).

61. Askerbeyli, R. T. T. and Askerzade, I. N., "BCS Superconductivity of Dirac Electrons in Graphene Monolayer", ***Journal Of Superconductivity And Novel Magnetism***, 32 (7): 1871–1874 (2019).

62. Solaimani, M., Cheraghi, F., and Nejati, M., "Effect of Geometry on the Electromagnetic Wave Transport Properties of Dielectric/Non-magnetized Plasma Photonic Crystals: Comparison of Top-Flat and Top-Curved Refractive Index Profiles", ***Optical And Quantum Electronics***, 54 (9): 581 (2022).

63. Vasconcelos, M. S. and Cottam, M. G., "Surface and bulk plasmon-polaritons in semiconductor photonic crystals with embedded graphene sheets", ***Journal Of Physics D: Applied Physics***, 52 (28): 285104 (2019).
64. Silva, E. F., Vasconcelos, M. S., Costa, C. H., Anselmo, D. H. A. L., and Mello, V. D., "Effects of graphene on light transmission spectra in Dodecanacci photonic quasicrystals", ***Optical Materials***, 98: 109450 (2019).

65. Costa, C. H., Vasconcelos, M. S., Fulco, U. L., and Albuquerque, E. L., "Thermal radiation in one-dimensional photonic quasicrystals with graphene", ***Optical Materials***, 72: 756–764 (2017).

66. Fan, Y., Wei, Z., Li, H., Chen, H., and Soukoulis, C. M., "Photonic band gap of a graphene-embedded quarter-wave stack", ***Physical Review B***, 88 (24): 241403 (2013).

## RESUME

Hiba ELHARKATI .She studied high school at Ibn Mandour School in Casablanca, majoring in Technical Sciences with a French option, and graduated at 2018. After that, she attended university at the Faculty of Science and Technology in Nouakchott, Mauritania, where she studied Physical Sciences and graduated in 2021. Subsequently, she studied language for a year in Turkey and graduated in 2022. Then, she started her master's studies in Physical Sciences at Karabuk University in Turkey and completed her Masters in Physics at 2024.